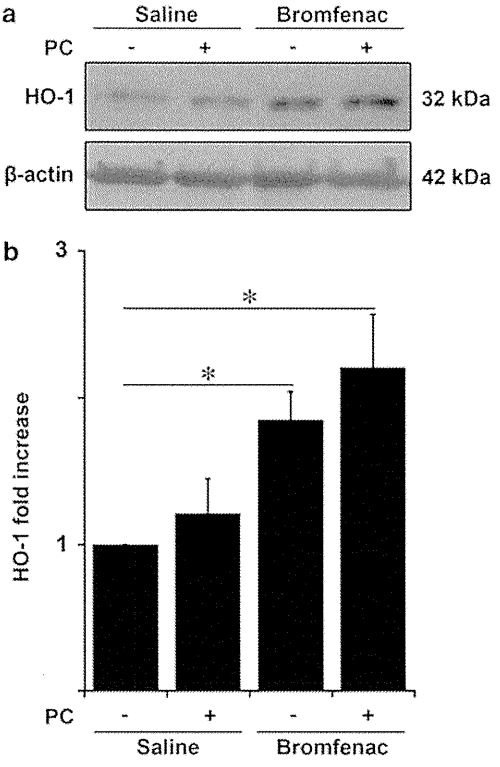

Figure 6 Western blot analysis of HO-1 in cytosolic proteins of rat retina–choroid homogenates. (**a**) Western blot shows HO-1 was upregulated with bromfenac and it was also slightly upregulated in eyes that received photocoagulation (PC) compared with others. (**b**) An analysis using densitometry on five independent western blots confirmed upregulation of HO-1 in bromfenac-treated eyes and photocoagulated eyes. Expressions of HO-1 in saline-treated eyes with no PC were defined as the base line, and fold increases of HO-1 in other eyes were calculated. Topical bromfenac significantly upregulated HO-1 expression (*$P<0.01$), and bromfenac-treated eyes with PC expressed more significant HO-1 expression (*$P<0.01$) compared with saline-treated eyes. Although not statistically significant, PC itself slightly upregulated HO-1 expression. The corrected significant *P*-value (Mann–Whitney *U*-test) was defined as 0.0125 (0.05/4 comparisons) after Bonferroni correction. Data were expressed as mean ± s.e.m.

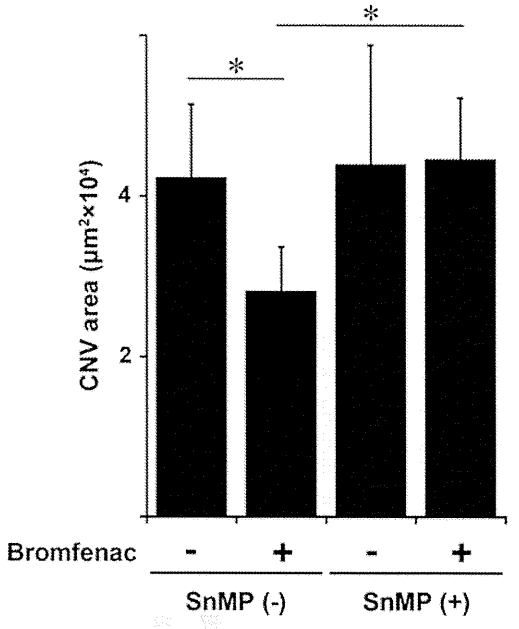

Figure 7 Effects of SnMP on inhibition of bromfenac over CNV size were studied. Topical bromfenac decreased the size of CNV compared with the control (bromfenac rat *vs* control rat. *$P<0.001$ or bromfenac rat *vs* bromfenac + SnMP rat; *$P<0.001$). This inhibitory effect was diminished by an inhibitor of HO-1 SnMP (control rat *vs* bromfenac + SnMP rats; $P=0.923$). On the other hand, SnMP itself did not have any significant effect on CNV size. The corrected significant *P*-value (Mann–Whitney *U*-test) was defined as 0.0125 (0.05/4 comparisons) after Bonferroni correction. $n=20$ (PC spots of five rats). Data were expressed as mean ± s.e.m.

protects retinal cells from light- or oxidant stress-induced cell death through the induction of HO-1.[44] Overexpression of HO-1 by gene transfer also inhibited light-induced photoreceptor cell apoptosis through Bcl-2 upregulation.[45] There are other reports showing that the induction of HO-1 by various stimulants rescued the retina in an ischemia-reperfusion model.[46] Therefore, NSAIDs might be beneficial for the treatment of CNV beyond their anti-angiogenic effect. This is especially true for the treatment of diseases of central nervous tissue including eye. At present, regeneration of neural tissue is clinically still difficult. Even if angiogenesis were to be blocked by an anti-VEGF drug, it would not necessarily mean the tissue function is protected. We need a potent angiogenesis therapy, but it must protect the host tissue as well. NSAIDs might be reasonable candidate drugs for this purpose.

It should be noted that there are other mechanisms to protect the retina from oxidative stress. Qin *et al*[47] showed that cyclopentenone 15-deoxy-delta^{12,14}-prostaglandin J2 protects RPE cells from oxidative injury. Although this mechanism is not evaluated in the present study, it is highly probable that these factors as a whole resulted in the present phenomenon.

There are different kinds of NSAIDs available. Each has different characteristics related to ocular penetration and inhibitory activity of COXs. For example, topical administration of 0.1% nepafenac inhibits the synthesis of PGs in the retina–choroid by 55% for 4 h.[48] Although, topical bromfenac has good ocular penetration and reaches a sufficient level in the retina and choroid, the inhibitory activity of bromfenac on either COX-1 or COX-2 was stronger than nepafenac or dicrofenac.[49,50] In our pilot study, we tested several different NSAIDs and found that topical bromfenac had a sufficient inhibitory effect on CNV in rat, as expected. Therefore, we chose bromfenac for the present study. But, it should be noted that the present results can be applied to bromfenac.

The present study has limitations. The present CNV model does not perfectly reflect clinical conditions. Certainly AMD or high myopia is a chronic and long-lasting disease. On the other hand, the present model is an acute wound-healing

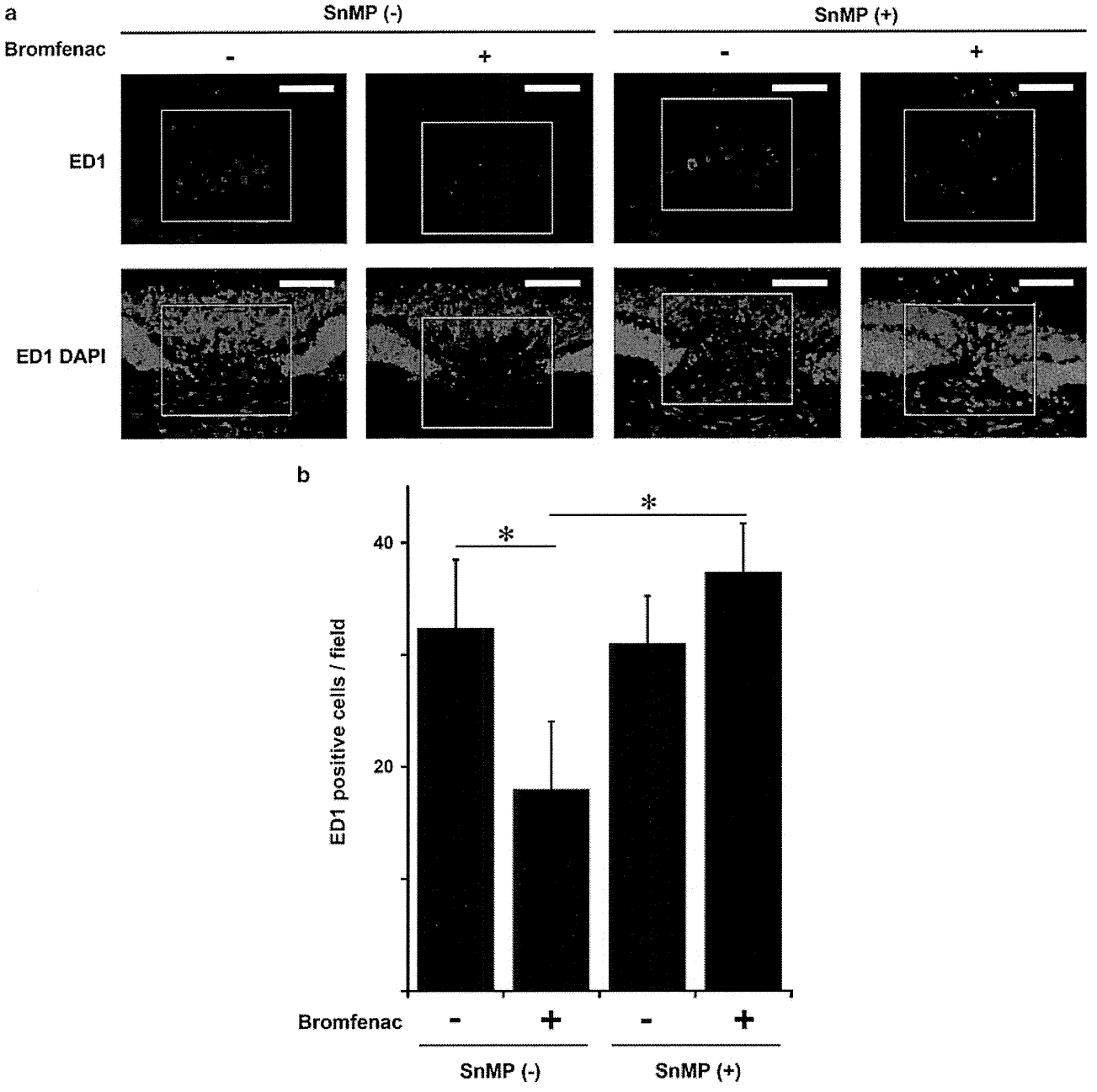

Figure 8 The number of infiltrating ED1-positive macrophages in CNV lesions was examined. (**a**) Representative images of rat CNV lesion identified by immunofluorescence with anti-ED1 antibody (red) and DAPI (blue). Scale bars: 150 μm (**b**). The number of ED1-positive macrophage infiltration expressed mean ± s.e.m. cells/field. In the group that received intraperitoneal PBS, infiltration of macrophage was decreased more significantly in bromfenac-treated rats than saline-treated rats ($^*P<0.01$). Intraperitoneal injections of SnMP reversed this effect and significantly increased macrophage infiltration ($^*P<0.01$). There was no significant change with macrophage infiltration in saline eye drop-treated rats ($P=0.074$). $n=10$. The corrected significant *P*-value (Mann–Whitney *U*-test) was defined as 0.0125 after Bonferroni correction. Square indicates CNV lesion.

model rather than a chronic disease model. Nonetheless, CNV in humans occurs in a similar manner to angiogenesis processes in acute wound healing and the present results will help an understanding of the clinical CNV. The second is that we measured the protein level of HO-1, but not its activity. The amount of protein does not necessarily reflect its biological activity. But the fact that an inhibitor of HO-1 reversed the effects of bromfenac indicates that HO-1 is likely to have played a major role in inhibiting CNV by bromfenac. The third is the treatment efficacy of NSAIDs. The current intravitreous anti-VEGF therapy is so potent for inhibiting CNV that there may be concerns that any new treatment will hardly improve on the current anti-VEGF therapy. However, complete blocking of VEGF might be potentially harmful

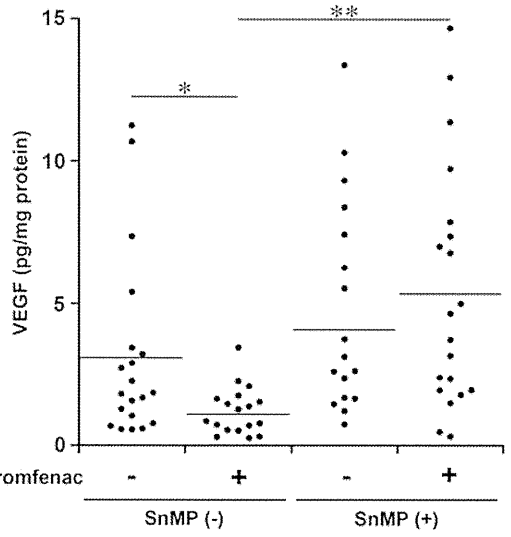

Figure 9 VEGF level of intraocular fluid in each eye was plotted. Analysis of intraocular fluid using ELISA showed that intraocular VEGF level was lower in bromfenac-treated rat ($*P<0.01$). Additional injection of SnMP increased intraocular VEGF level as high as in control CNV rats ($**P<0.001$). No significant difference resulted from intraperitoneal SnMP alone. Each group contained 20 samples from 20 eyes ($n=20$). Mean value of each group was expressed by a line. The corrected significant *P*-value (Mann–Whitney *U*-test) was defined as 0.0125 after Bonferroni correction.

after a long period.[7,10] Topical NSAIDs had therapeutic effects on CNV in this study. Because it has such a potentially neuroprotective effect, combination therapy with an anti-VEGF drug may be very advantageous for patients. Combination therapy is found to be more effective, but is less likely to result in drug resistance than mono-therapy in the t reatment of tumor angiogenesis.[51] In addition, repeated intravitreal injections were necessary for the majority of patients to maintain this level of benefit.[4,5] Intravitreal injections can be physically uncomfortable, and they expose the patient to a number of potential vision-threatening complications such as intraocular infection. Topical administration of a drug that has the capacity to substantially reduce CNV would be a promising advance in the development of therapies for neovascular eye diseases. Finally, there was a technical problem in this study. RT-PCR might be more suitable for objective quantification of invading macrophages. We performed RT-PCR using a primer for macrophage; however, no reproducible data were obtained (data not shown). The results were strongly affected by the size of photocoagulation spot or sampling biases. This limitation should be also noted.

In conclusion, the present study showed a new mechanism of NSAIDs for inhibiting neovascularization of the choroid. Topical NSAIDs would be beneficial for the treatment of CNV not only because of its anti-angiogenic effect but also its potential anti-stress effect. Because the CNV model can be a mirror for other angiogenic diseases in the central nervous system, NSAIDs could be studied more widely and profoundly as a candidate therapy for these disease conditions (Supplementary Figure 1).

Supplementary Information accompanies the paper on the Laboratory Investigation website (http://www.laboratoryinvestigation.org)

ACKNOWLEDGEMENTS

This work was supported by a grant from the Research Committee on Chorioretinal Degeneration and Optic Atrophy, Ministry of Health, Labor, and Welfare, Tokyo, Japan; and by a Grant-in-Aid for Scientific Research from the Ministry of Education, Science, and Culture of the Japanese Government, Tokyo, Japan.

DISCLOSURE/CONFLICT OF INTEREST

The authors declare no conflict of interest.

1. Bressler NM, Bressler SB, Fine SL. Age-related macular degeneration. Surv Ophthalmol 1988;32:375–413.
2. Soubrane G. Choroidal neovascularization in pathologic myopia: recent developments in diagnosis and treatment. Surv Ophthalmol 2008;53:121–138.
3. Cohen SY, Laroche A, Leguen Y, *et al.* Etiology of choroidal neovascularization in young patients. Ophthalmology 1996;103: 1241–1244.
4. TAP study group. Photodynamic therapy of subfoveal choroidal neovascularization in age-related macular degeneration with verteporfin: one-year results of 2 randomized clinical trials–TAP report. Treatment of age-related macular degeneration with photodynamic therapy (TAP) Study Group. Arch Ophthalmol 1999;117:1329–1345.
5. Rosenfeld PJ, Brown DM, Heier JS, *et al.* Ranibizumab for neovascular age-related macular degeneration. N Engl J Med 2006;355:1419–1431.
6. Nishijima K, Ng YS, Zhong L, *et al.* Vascular endothelial growth factor-A is a survival factor for retinal neurons and a critical neuroprotectant during the adaptive response to ischemic injury. Am J Pathol 2007;171:53–67.
7. Robinson GS, Ju M, Shih SC, *et al.* Nonvascular role for VEGF: VEGFR-1, 2 activity is critical for neural retinal development. FASEB J 2001;15:1215–1217.
8. Murakami Y, Ikeda Y, Yonemitsu Y, *et al.* Inhibition of choroidal neovascularization via brief subretinal exposure to a newly developed lentiviral vector pseudotyped with Sendai viral envelope proteins. Hum Gene Ther 2010;21:199–209.
9. Saint-Geniez M, Kurihara T, Sekiyama E, *et al.* An essential role for RPE-derived soluble VEGF in the maintenance of the choriocapillaris. Proc Natl Acad Sci USA 2009;106:18751–18756.
10. Rosenfeld PJ, Shapiro H, Tuomi L, *et al.* Characteristics of patients losing vision after 2 years of monthly dosing in the phase III ranibizumab clinical trials. Ophthalmology 2011;118:523–530.
11. Sakamoto T, Soriana D, Nassaralla J, *et al.* Effect of intravitreal administration of indomethacin on experimental subretinal neovascularization in the subhuman primate. Arch Ophthalmol 1995; 113:222–226.
12. Takahashi H, Yanagi Y, Tamaki Y, *et al.* COX-2-selective inhibitor, etodolac, suppresses choroidal neovascularization in a mice model. Biochem Biophys Res Commun 2004;325:461–466.
13. Takahashi K, Saishin Y, Saishin Y, *et al.* Topical nepafenac inhibits ocular neovascularization. Invest Ophthalmol Vis Sci 2003;44:409–415.
14. Yanni SE, Clark ML, Yang R, *et al.* The effects of nepafenac and amfenac on retinal angiogenesis. Brain Res Bull 2010;81:310–319.
15. Kim SJ, Toma HS. Inhibition of choroidal neovascularization by intravitreal ketorolac. Arch of Ophthalmol 2010;128:596–600.
16. Kim SJ, Toma HS, Barnett JM, Penn JS. Ketorolac inhibits choroidal neovascularization by suppression of retinal VEGF. Exp Eye Res 2010;91:537–543.
17. Wilson HL, Schwartz DM, Bhatt HR, *et al.* Statin and aspirin therapy are associated with decreased rates of choroidal neovascularization among patients with age-related macular degeneration. Am J Ophthalmol 2004;137:615–624.

18. Rezaei KA, Toma H, Cai J, *et al.* Reduced choroidal neovascular membrane formation in cyclooxygenase-2 null mice. Invest Ophthalmol Vis Sci 2010;52:701–707.
19. Tegeder I, Pfeilschifter J, Geisslinger G. Cyclooxygenase-independent actions of cyclooxygenase inhibitors. FASEB J 2001;15:2057–2072.
20. Ponka P. Cell biology of heme. Am J Med Sci 1999;318:241–256.
21. Maines MD. The heme oxygenase system: a regulator of second messenger gases. Annu Rev Pharmacol Toxicol 1997;37:517–554.
22. Brouard S, Otterbein LE, Anrather J, *et al.* Carbon monoxide generated by heme oxygenase 1 suppresses endothelial cell apoptosis. J Exp Med 2000;192:1015–1026.
23. Alcaraz MJ, Habib A, Créminon C, *et al.* Heme oxygenase-1 induction by nitric oxide in RAW 264.7 macrophages is upregulated by a cyclooxygenase-2 inhibitor. Biochim Biophys Acta 2001;1526:13–16.
24. Hou CC, Hung SL, Kao SH, *et al.* Celecoxib induces heme-oxygenase expression in glomerular mesangial cells. Ann NY Acad Sci 2005; 1042:235–245.
25. Nascimento-Silva V, Arruda MA, Barja-Fidalgo C, *et al.* Novel lipid mediator aspirin-triggered lipoxin A4 induces heme oxygenase-1 in endothelial cells. Am J Physiol Cell Physiol 2005;289:C557–C563.
26. Grosser N, Abate A, Oberle S, *et al.* Heme oxygenase-1 induction may explain the antioxidant profile of aspirin. Biochem Biophys Res Commun 2003;308:956–960.
27. Cantoni L, Valaperta R, Ponsoda X, *et al.* Induction of hepatic heme oxygenase-1 by diclofenac in rodents: role of oxidative stress and cytochrome P-450 activity. J Hepatol 2003;38:776–783.
28. Arimura N, Ki-i Y, Hashiguchi T, *et al.* Intraocular expression and release of high-mobility group box 1 protein in retinal detachment. Lab Invest 2009;89:278–289.
29. Otsuka H, Arimura N, Sonoda S, *et al.* Stromal cell-derived factor-1 is essential for photoreceptor cell protection in retinal detachment. Am J Pathol 2010;177:2268–2277.
30. Fujimoto T, Sonoda KH. Choroidal neovascularization enhanced by Chlamydia pneumoniae via Toll-like receptor 2 in the retinal pigment epithelium. Invest Ophthalmol Vis Sci 2010;51:4694–4702.
31. Honda M, Sakamoto T, Ishibashi T, *et al.* Experimental subretinal neovascularization is inhibited by adenovirus-mediated soluble VEGF/flt-1 receptor gene transfection: a role of VEGF and possible treatment for SRN in age-related macular degeneration. Gene Ther 2000;7:978–985.
32. Aburaya M, Tanaka K-I, Hoshino T, *et al.* Heme oxygenase-1 protects gastric mucosal cells against non-steroidal anti-inflammatory drugs. J Biol Chem 2006;281:33422–33432.
33. Jones MK, Wang H, Peskar BM, *et al.* Inhibition of angiogenesis by nonsteroidal anti-inflammatory drugs: insight into mechanisms and implications for cancer growth and ulcer healing. Nat Med 1999;5: 1418–1423.
34. Jones MK, Szabó IL, Kawanaka H, *et al.* von Hippel Lindau tumor suppressor and HIF-1alpha: new targets of NSAIDs inhibition of hypoxia-induced angiogenesis. FASEB J 2002;16:264–266.
35. Ferrara N. Vascular endothelial growth factor and the regulation of angiogenesis. Recent Prog Horm Res 2000;55:15–35.
36. Tsutsumi C, Sonoda KH, Egashira K, *et al.* The critical role of ocular-infiltrating macrophages in the development of choroidal neovascularization. J Leukoc Biol 2003;74:25–32.
37. Ghosh S, May MJ, Kopp EB. NF-kappa B and Rel proteins: evolutionarily conserved mediators of immune responses. Annu Rev Immunol 1998;16:225–260.
38. Jaiswal AK. Nrf2 signaling in coordinated activation of activation of antioxidant gene expression. Free Radic Biol Med 2004;36: 1199–1207.
39. Kaspar JW, Niture SK, Jaiswal AK. Nrf2:INrf2 (Keap1) signaling in oxidative stress. Free Radic Biol Med 2009;47:1304–1309.
40. Healy ZR, Lee NH, Gao X, *et al.* Divergent responses of chondrocytes and endothelial cells to shear stress: cross-talk among COX-2, the phase 2 response, and apoptosis. Proc Natl Acad Sci USA 2005;102: 14010–14015.
41. Bussolati B, Ahmed A, Pemberton H, *et al.* Bifunctional role for VEGF-induced heme oxygenase-1 *in vivo*: induction of angiogenesis and inhibition of leukocytic infiltration. Blood 2004;103:761–766.
42. Dulak J, Loboda A, Zagórska A, Józkowicz A. Complex role of heme oxygenase-1 in angiogenesis. Antioxid Redox Signal 2004;6: 858–866.
43. Bussolati B, Mason JC. Dual role of VEGF-induced heme-oxygenase-1 in angiogenesis. Antioxid Redox Signal 2006;8:1153–1163.
44. Mandal MN, Patlolla JM, Zheng L, *et al.* Curcumin protects retinal cells from light-and oxidant stress-induced cell death. Free Radic Biol Med 2009;46:672–679.
45. Shyong MP, Lee FL, Hen WH, *et al.* Viral delivery of heme oxygenase-1 attenuates photoreceptor apoptosis in an experimental model of retinal detachment. Vision Res 2008;48:2394–2402.
46. Sun MH, Su Pang JH, Chen SL, *et al.* Retinal protection from acute glaucoma-induced ischemia-reperfusion injury through pharmacological induction of heme oxygenase-1 by cobalt protoporphyrin. Invest Ophthalmol Vis Sci 2010;51:4798–4808.
47. Qin S, McLaughlin AP, De Vries GW. Protection of RPE cells from oxidative injury by 15-deoxy-delta12,14-prostaglandin J2 by augmenting GSH and activating MAPK. Invest Ophthalmol Vis Sci 2006;47: 5098–5105.
48. Gamache DA, Graff G, Brady MT, *et al.* Nepafenac, a unique non-steroidal prodrug with potential utility in the treatment of trauma-induced ocular inflammation. I: assessment of anti-inflammatory efficacy. Inflammation 2000;24:357–370.
49. Isaka M, Inada K, Tsutsumi S, *et al.* Ocular tissue distribution in rabbit after instillation of bromfenac sodium ophthalmic solution. Drug Metabol Pharmacokinet 1999;14:32–41.
50. Kida T, Ogawa T, McNamara TR, *et al.* Evaluations of the human COX-1 and COX-2 inhibition for amfenac, bromfenac, ciclofenac, and ketorolac. Annu Meet Guide Abstr Am Coll Clin Pharm 2007; (Suppl):274.
51. Abdollahi A, Folkman J. Evading tumor evasion: current concepts and perspectives of anti-angiogenic cancer therapy. Drug Resist Updat 2010;13:16–28.

Q5

Autofluorescence of the Cells in Human Subretinal Fluid

Tetsuju Sekiryu,[1] *Yasuharu Oguchi,*[1] *Seisuke Arai,*[2] *Ikuo Wada,*[2] *and Tomohiro Iida*[1]

Purpose. The origin of autofluorescence in the subretinal space and the autofluorescence properties of the cells were investigated in surgically collected subretinal fluid.

Methods. Subretinal fluid was surgically collected from four eyes of patients with rhegmatogenous retinal detachment (three eyes) and Coats' disease (one eye). After cytocentrifuge preparation of the cells in the fluid and immunofluorescence staining, a cytologic examination was conducted by using confocal scanning laser microscopy. The autofluorescence of the cells was elucidated by measuring the fluorescence spectra with spectroscopy, to obtain different excitation laser light emission fingerprints.

Results. The cells from the subretinal fluid were classified into three types: CD68-negative cells containing numerous pigmented granules, CD68-positive cells containing few pigments, and CD68-negative cells with no pigmented granules. Autofluorescence was observed in the inclusions of the cells classified into the former two types. When the cells were excited by a 458- or 488-nm laser light, emission spectra in autofluorescence showed little difference between CD68-positive and -negative cells. Peak analysis confirmed that the two types of cells showed the same emission peaks within this range of excitation light.

Conclusions. Autofluorescent inclusions appeared in the CD68-positive and -negative cells in the subretinal fluid. The macrophages in the subretinal fluid possess autofluorescence that is spectroscopically similar to lipofuscin. Autofluorescence of macrophages can be attributed to degenerated outer segments and debris from apoptotic photoreceptors. Clinicians should consider migration of macrophages, in addition to retinal pigment epithelium, as the possible source when abnormal fundus autofluorescence is observed using an ordinary set of fluorescence filters. (*Invest Ophthalmol Vis Sci.* 2011;52: 8534–8541) DOI:10.1167/iovs.11-8012

Fundus autofluorescence (FAF) mainly originates from lipofuscin in the retinal pigment epithelium. Recent studies revealed that a main constituent of lipofuscin that generates autofluorescence is pyridinium bisretinoid (A2E).[1–3] The derivatives of A2E in the photoreceptor outer segments are considered to be another source of abnormal FAF. Novel imaging technology of FAF and optical coherence tomography demonstrated subretinal autofluorescent deposits in some macular diseases with serous retinal detachment, such as vitelliform macular dystrophy,[4,5] central serous chorioretinopathy,[6–11] choroidal melanoma,[12] and Vogt-Koyanagi-Harada disease.[13] Various materials or cells have been proposed as the origin of autofluorescent deposits. These include migrating retinal pigment epithelial cells, debris of degenerated photoreceptor outer segments, or macrophages that have phagocytosed the outer segments. Among them, macrophages are thought to be the main source of the subretinal autofluorescent deposits.[14] Migrating macrophages in the subretinal space are often found in histopathologic specimens and surgically excised tissue from patients with several retinal diseases, such as Best's vitelliform macular dystrophy,[15,16] age-related macular degeneration,[17,18] macular holes,[19] rhegmatogenous retinal detachment (RRD),[20,21] and Coats' disease.[21,22] However, it is not clearly demonstrated that macrophages are the source of autofluorescence in the subretinal space. In the present study, we investigated surgically collected cells in the subretinal fluid and characterized the fluorescence properties of the cells.

Methods

This study complied with the Declaration of Helsinki. The institutional review board at Fukushima Medical University School of Medicine approved: (1) observation using optical coherence tomography and FAF in eyes with macular and retinal disorders and the retrospective comparative analysis performed in this study and (2) biochemical or histopathologic examination of tissues and fluid collected from the eyes at the time of surgery. Written informed consent was obtained from all patients.

Subretinal fluid from four eyes of four patients who had retinal detachment was examined. All four eyes showed hyperautofluorescence in the area of retinal detachment. Three eyes with long-standing RRD and one eye with Coats' disease underwent a routine ophthalmic examination, including determination of best corrected visual acuity (BCVA), intraocular pressure, slit lamp biomicroscopy with a contact lens, and fundus color photography. Fundus autofluorescence was taken with a confocal laser scanning ophthalmoscope (HRA2; Heidelberg Engineering, Heidelberg, Germany) using 488-nm excitation laser and a barrier filter at 500 nm.

Fluid Collection

Subretinal fluid was collected during surgery for retinal detachment. All three eyes with RRD were treated with a scleral buckling procedure. The subretinal fluid was aspirated with a blunt needle attached to a sterilized syringe and introduced into the site of scleral puncture for subretinal fluid drainage. The cryopexy was always performed after subretinal fluid drainage. Specimens with blood contamination were discarded. The eye with Coats' disease was treated with vitrectomy. After aspiration of the crystalline lens and core vitrectomy, an intentional tear was made in the upper temporal quadrant by intraocular diathermy. During fluid–air exchange for retinal reattachment, the subretinal fluid was passively aspirated from the intentional tear into a sterilized syringe. Retinal photocoagulation around the intentional tear and the area of retinal vascular abnormality was made after reattachment of the retina. All four eyes were reattached after a single surgery.

From the Departments of [1]Ophthalmology and [2]Cell Science, Fukushima Medical University School of Medicine, Fukushima, Japan.

Submitted for publication June 9, 2011; revised August 23 and September 21, 2011; accepted September 21, 2011.

Disclosure: **T. Sekiryu**, None; **Y. Oguchi**, None; **S. Arai**, None; **I. Wada**, None; **T. Iida**, None

Corresponding author: Tetsuju Sekiryu, Department of Ophthalmology, Fukushima Medical University School of Medicine, 1 Hikarigaoka, Fukushima City, Fukushima, 960-1295, Japan; sekiryu@fmu.ac.jp.

Investigative Ophthalmology & Visual Science, October 2011, Vol. 52, No. 11

TABLE 1. Clinical Features of the Patients

Patient	Age	Sex	Disease	Subretinal Deposits	Subretinal Strand	Duration of Retinal Detachment	FAF
Patient 1	11	Male	RRD	+	+	unknown	Granular
Patient 2	17	Male	RRD	+	+	4.5M	Granular
Patient 3	24	Male	RRD	+	+	6M	Granular
Patient 4	15	Male	Coats' disease	+	+	4M	Diffuse

Fluorescence Spectroscopy

Collected subretinal fluid was cytocentrifuged (GP centrifuge; Beckman, Fullerton, CA) onto a glass slide coated with poly-L-lysine (P4832; Sigma-Aldrich, St. Louis, MO) at the bottom of a 24-well multiwell plate (BD Falcon, Bedford, MA) at 1500 rpm for 10 minutes. Supernatant was removed. Subsequently, the cells were incubated at 37°C in RPMI 1640 medium containing 10% FBS. After incubation for 3 hours, the cells were washed three times with PBS and fixed in acetone/methanol (2:3) for 10 minutes at −20°C. After blocking nonspecific protein in 0.1% BSA in PBS for 30 minutes at room temperature, primary antibody CD68 (ab845; Abcam, Cambridge, UK) was applied for 3 hours at room temperature, and secondary antibody (Alexa Fluor 647; Invitrogen, Carlsbad, CA) was applied for 30 minutes at room temperature. The negative control was without secondary antibody. Immunofluorescence-labeled and differential interference images were obtained (LSM510 META; Carl Zeiss Meditec, Dublin, CA). The emission fingerprint of fluorescence was also recorded using the lambda META scanning mode, in which fluorescence in a 10-nm width is recorded by a polychromatic 8-channel detector that allows fast acquisition of lambda stacks. Fluorescence was excited by an Ar^+ laser for 458, 488, and 514 nm; an HeNe laser for 532 nm excitation; and an HeNe laser for 633-nm excitation through an appropriate dichroic mirror. To compare the emission fingerprint, the detector gain and excitation light intensity were set constant for a set of experiments. The fluorescence intensity profile was exported as text and used to analyze the peak, by using the local maximum method in the peak-finding module of the software (Origin 8; OriginLab Corp., Northampton, MA).

RESULTS

Identification of Cells

The ages of the patients with RRD were 11, 17, and 24 years (Table 1). Preoperative examination revealed yellow precipitates and corresponding granular autofluorescence on the outer surface of the retina in all three eyes with long-standing RRD. All eyes with retinal detachment had subretinal strands that showed hyperautofluorescence (Fig. 1). The eye with Coats' disease in a 15-year-old boy showed diffuse hyperautofluorescence in the area of bullous retinal detachment. Part of hyperautofluorescence appeared as spotted hyperautofluorescent lesions between the retinal folds (Fig. 2).

The cells from the subretinal space were classified into three types. The first type was relatively large, round cells that had

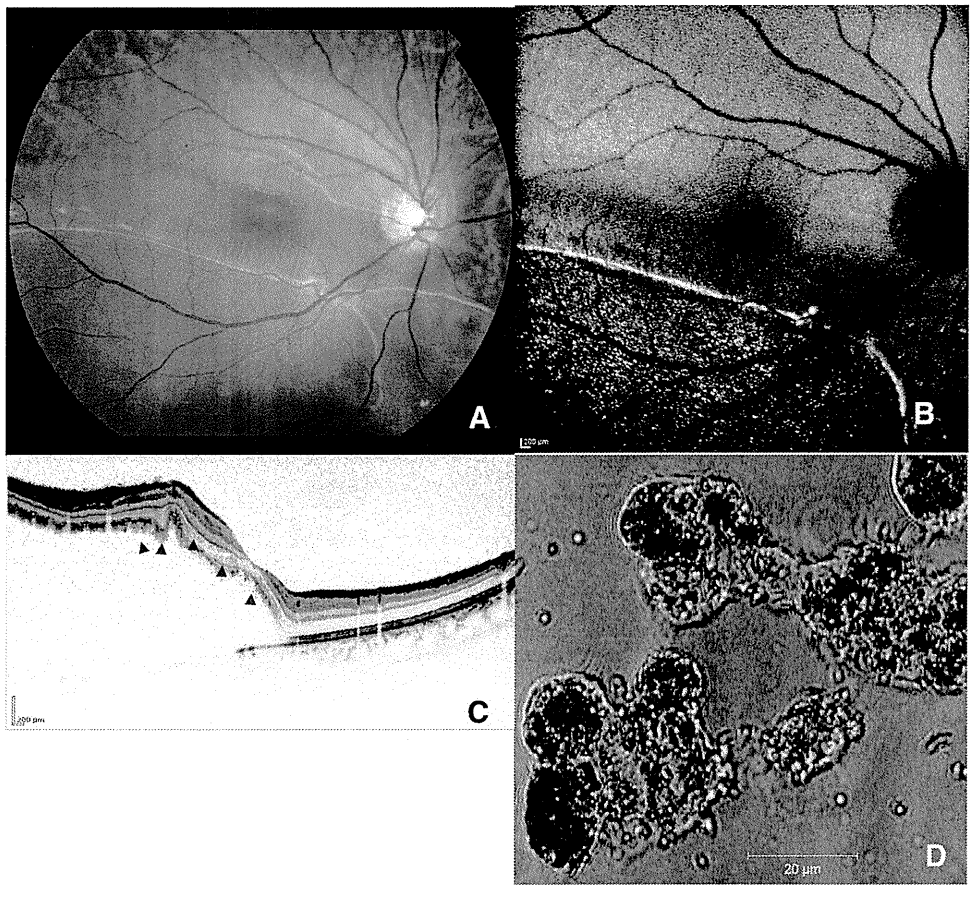

FIGURE 1. A 24-year-old man. The right eye showed long-standing retinal detachment with a subretinal strand (**A**). FAF demonstrated granular hyperautofluorescence within retinal detachment (**B**). The subretinal strand also showed strong granular hyperautofluorescence. OCT revealed low signal intensity dots on the outer retinal surface or in the retina (*arrowheads*) (**C**). Differential interference image of the pigmented cells in subretinal fluid (**D**).

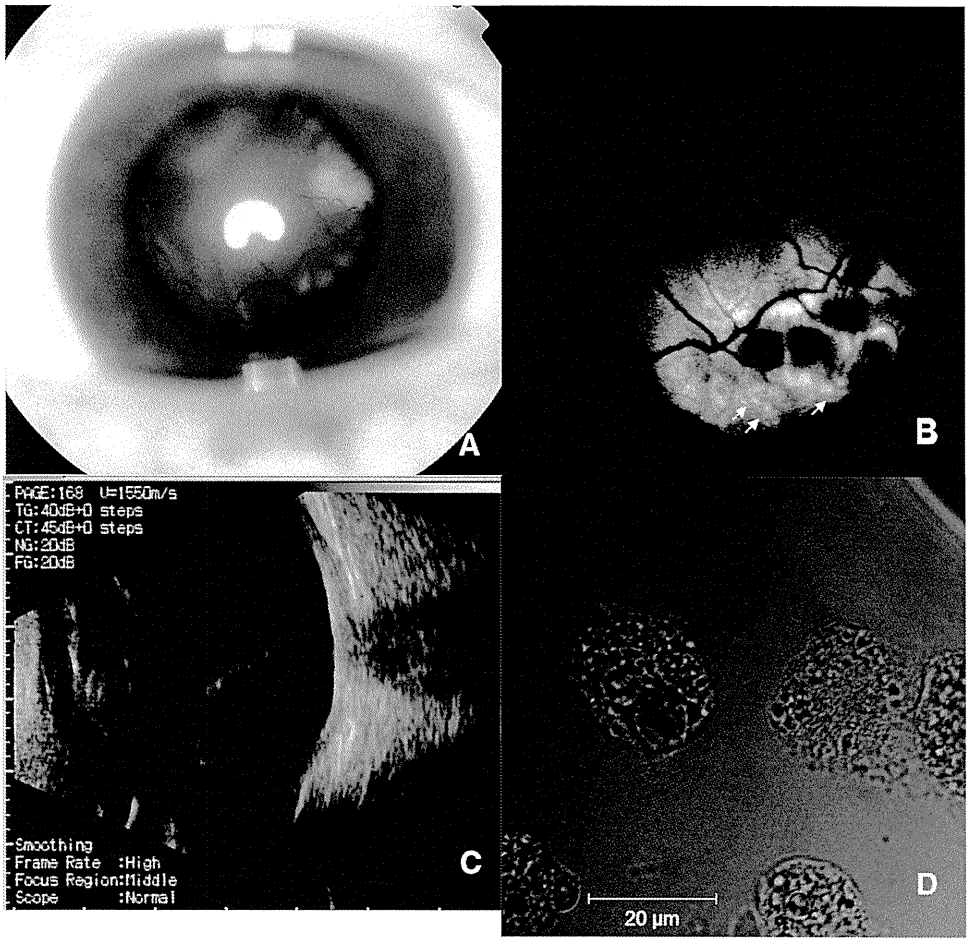

FIGURE 2. A 15-year-old boy. The left eye showed bullous retinal detachment with a yellow subretinal deposit (**A**). Fundus autofluorescence demonstrated diffuse hyperautofluorescence (**B**). Ultrasonography showed bullous retinal detachment (**C**). Large cells in the subretinal fluid with few pigment granules were observed by differential interference microscopy (**D**). Some spotted hyperautofluorescent lesions appeared between the retinal fold (*arrow*).

well-defined cytoplasm and nuclei covered with numerous pigments. Heavily pigmented cells were negative for CD68 staining. Autofluorescent inclusions appeared in the cytoplasm (Fig. 3). This type of cell frequently appeared in the specimens of the RRD cases. The second type was large (20–50 μm in diameter), rounded or polygonal cells with few or no pigments. Differential interference contrast microscopy showed various sizes of vacuoles in the cytoplasm. Most of the subretinal cells in the eye with Coats' disease were positive for CD68 staining (patient 4). The contour of vacuoles was clearly observed when the cells were stained immunocytochemically. Autofluorescent inclusions appeared in the cytoplasm and in some vacuoles (Fig. 4). This type of cell appeared more frequently in the specimens from the subretinal fluid of Coats' disease. The third type of cell is the spindle-shaped or oval cells that had few or no pigments in the cytoplasm. These cells were negative for CD68 staining and did not show autofluorescence. The density of each type of the cells was summarized in Figure 5.

Fluorescence Spectroscopy

Fluorescence spectroscopy was applied to the first two types of cells. The intensity of autofluorescence of inclusions in the cells with CD68-positive or -negative cells stained with anti-CD68 antibody probed by AlexaFluor-647-labeled secondary antibody was examined with various excitation lights (458, 488, 514, 543, and 633 nm). The cells were characterized by the presence of far-red to infrared fluorescence excited by a 633-nm laser (Figs. 6I, 6J). Unexpectedly, when excited by a 458- or 488-nm laser light, emission spectra of autofluorescence showed little difference, either in CD68-positive or -negative cells (Figs. 6A–D). The emission peak at 580 nm was comparable in either type of cell. Red fluorescence obtained by excitation with longer wavelengths (514 and 543 nm) was higher in CD68-positive cells (Figs. 6E–H), but the CD68-negative cells still showed significant autofluorescence. We could not find any remarkable difference in the spectra between the cells from the eyes with RRD and that from the eye with Coats' disease. To obtain quantitative information, peak analysis was performed for each emission curve on a total of 50 autofluorescent inclusions in four to six typical cells from each of the four specimens (Table 2). Consistent with Figure 6, this analysis also indicates that almost all CD68-negative cells contain apparent autofluorescent vesicles, demonstrating that autofluorescence does not associate with CD68 expression. In the 458- and 488-nm emission spectra, the cells classified as the former two types showed the narrow peak at the same wavelength.

DISCUSSION

Characteristics of autofluorescence were examined in the cells collected from subretinal fluid in eyes with retinal detachment, which showed autofluorescence in the area of retinal detachment. The cells were classified morphologically and immunocytologically, with CD68 used as the marker for macrophages. We found that autofluorescent inclusions appeared in the CD68-positive cells and -negative cells. No clear difference in autofluorescence spectra was observed in the two types of cells.

Although the main origin of FAF is lipofuscin in the retinal pigment epithelium, the subretinal deposits also show autofluorescence in eyes with retinal detachment caused by RRD,[22] central serous chorioretinopathy,[8,10,11,23] Best's disease,[4,24] age-related macular degeneration,[25] or choroidal hemangi-

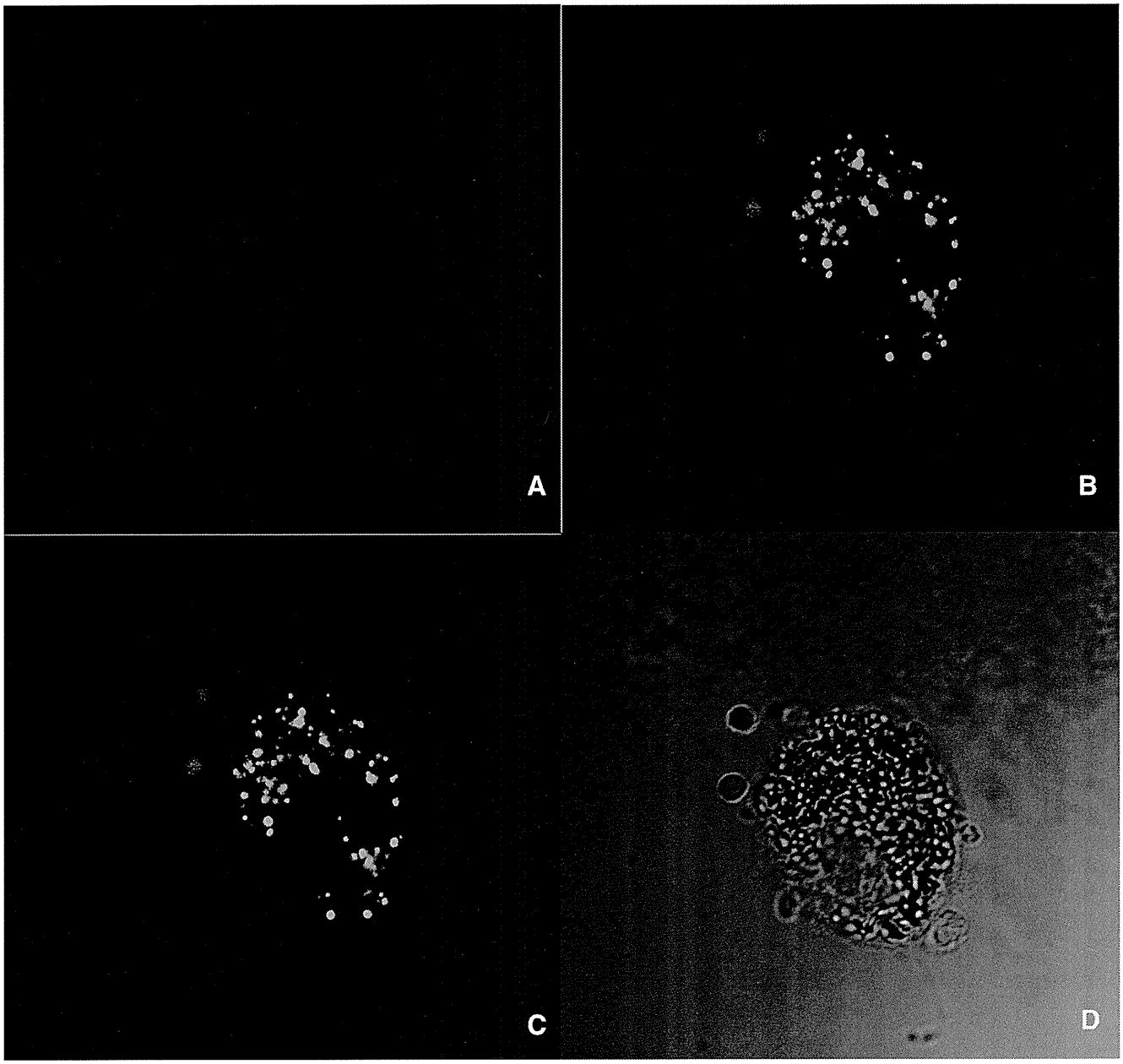

FIGURE 3. A cell obtained from the eye with rhegmatogenous retinal detachment shown in Figure 1 is negative for CD68 (**A**). Numerous small green autofluorescent inclusions in the cytoplasm were excited at 488 nm (**B**). (**A**) and (**B**) are superimposed in (**C**). The cytoplasm of the cell was filled with numerous pigment granules (**D**).

oma.[26] It has been speculated that the autofluorescent deposits may originate from macrophages.[8,10,14] However, little is known about autofluorescence of the macrophages in the subretinal space. In addition, although immunofluorescent staining of CD68 is frequently used as the cytomarker for macrophages in histologic study of the retina and the choroid, little information has been provided about autofluorescence of the CD68-positive cells in the eye. Thus, information about autofluorescence of the macrophages may help to interpret histologic results. In the present study, we investigated the autofluorescence properties of CD68-positive cells. AlexaFluor-647 was used as a secondary antibody dye to identify macrophages without interfering with observation of autofluorescence from the cells.

A case with subretinal precipitates in long-standing retinal detachment was reported by Vogt[27] in 1938. In such eyes, cytologic study has revealed that macrophages are the dominant cell population in the subretinal fluid.[28,29] Coats' disease is a retinal vascular disease showing yellow golden deposits in the retina[30] and bullous retinal detachment occasionally. Numerous macrophages were confirmed in the subretinal fluid aspirated from the eyes with retinal detachment.[21,31] Abnormal FAF in both diseases has not been reported. We noticed hyperautofluorescent deposits corresponding to subretinal precipitates in the eyes with RRD and spotted hyperautofluorescence in the area of retinal detachment caused by Coats' disease. In the eyes with RRD, hyperautofluorescence appeared along subretinal strands. Previous histopathologic studies suggested that subretinal strands are composed of macrophage and retinal pigment epithelium.[32–35] Macrophages may have a part in the origin of subretinal strands.

Three types of cells were morphologically identified in the subretinal fluid from the four eyes in the present study. Immuno-

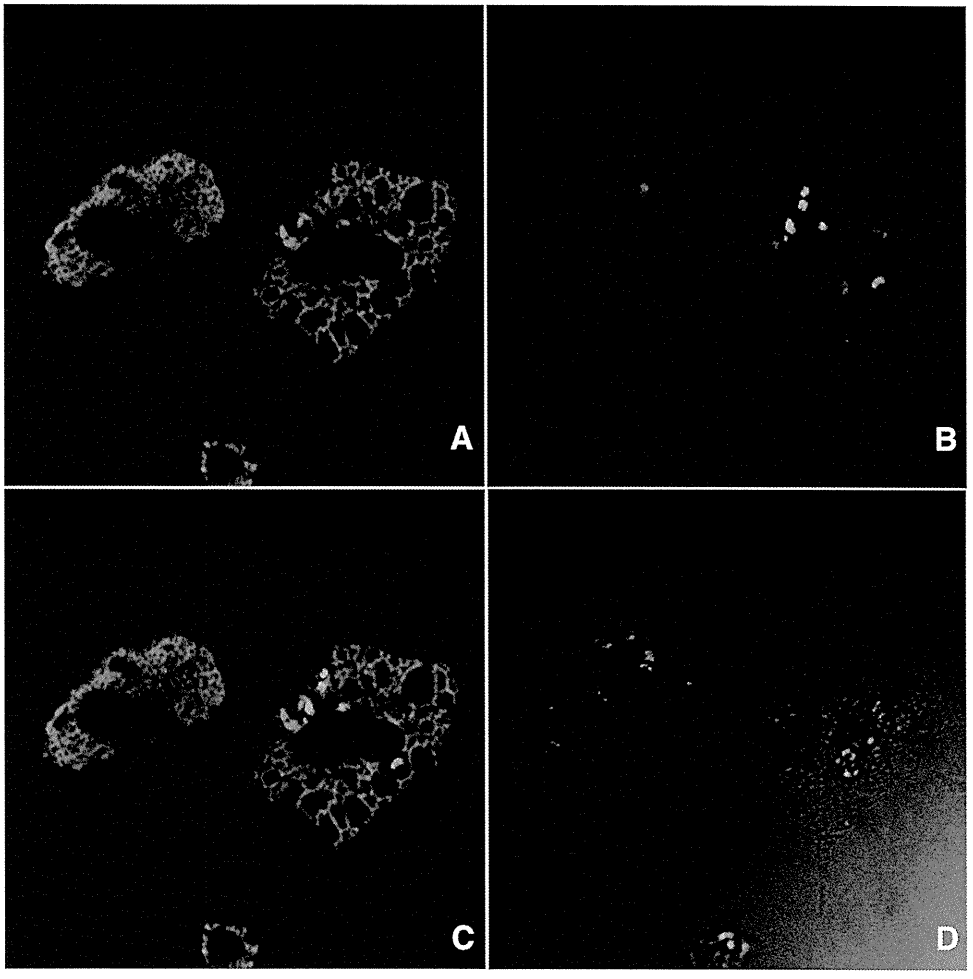

FIGURE 4. This cell was obtained from the eye with exudative retinal detachment shown in Figure 2. Polygonal large cells with numerous vacuoles were positive for CD68 (**A**). Green autofluorescent inclusions were excited by a 488-nm laser light (**B**). (**A**) and (**B**) are superimposed. Autofluorescent inclusions were observed in the vacuoles and cytoplasm (**C**). In some cells, few pigment granules were found (**D**).

fluorescent staining confirmed that most of the lightly pigmented large cells were CD68-positive macrophages. Pigmented CD68-negative cells, on the other hand, were considered likely to be derived from the retinal pigment epithelium, because of their morphologic characteristics. Since autofluorescence appeared only in these types of cells, they were possible origins of abnormal autofluorescence in the subretinal space.

Peak analysis for 50 inclusions consistently showed similar fluorescence properties, suggesting that the inclusions in both types of cells may have similar composition of fluorescent material. Autofluorescent inclusions in both types of cells showed yellow-red peak emissions within the range of 558 to 612 nm (Fig. 6). Consistent with this observation, ex vivo experiments of the human retinal pigment epithelium showed that the peak emission of lipofuscin appeared within the range of 588 to 610 nm.[36] Peak emission of lipofuscin varies by age,[25,37] physical condition,[38] and method of extraction. Consideration of variation of emission spectra of lipofuscin from these reports suggests that yellow-red emission originates from lipofuscin-like materials in the cells. Previously, lipofuscin was considered to be synthesized in the retinal pigment epithelium as a product of phagocytosis of the photoreceptor outer segments. Recent reports have suggested that A2E and its derivatives are synthesized in the photoreceptor outer segments before phagocytosis by the retinal pigment epithelium.[39] Lipofuscin-like materials could also accumu-

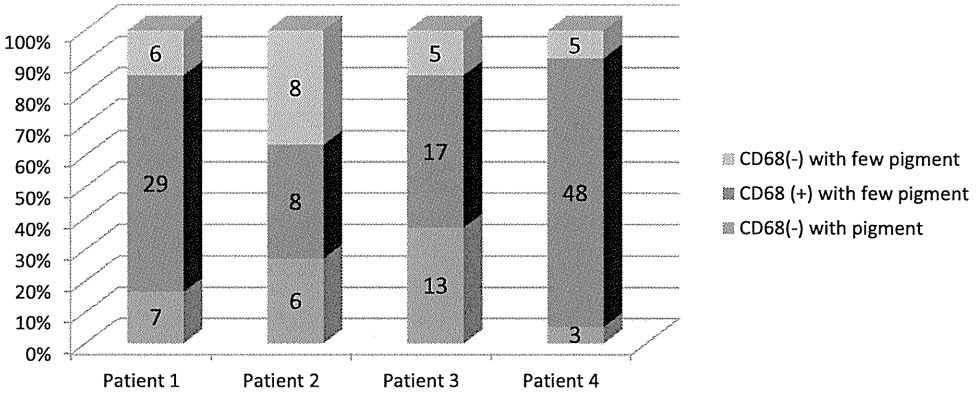

FIGURE 5. The cell density of each type of the cells. The number of cells in four microscopic fields when 40× object lens was used. Total area of counting cells was approximately 0.1024 mm^3.

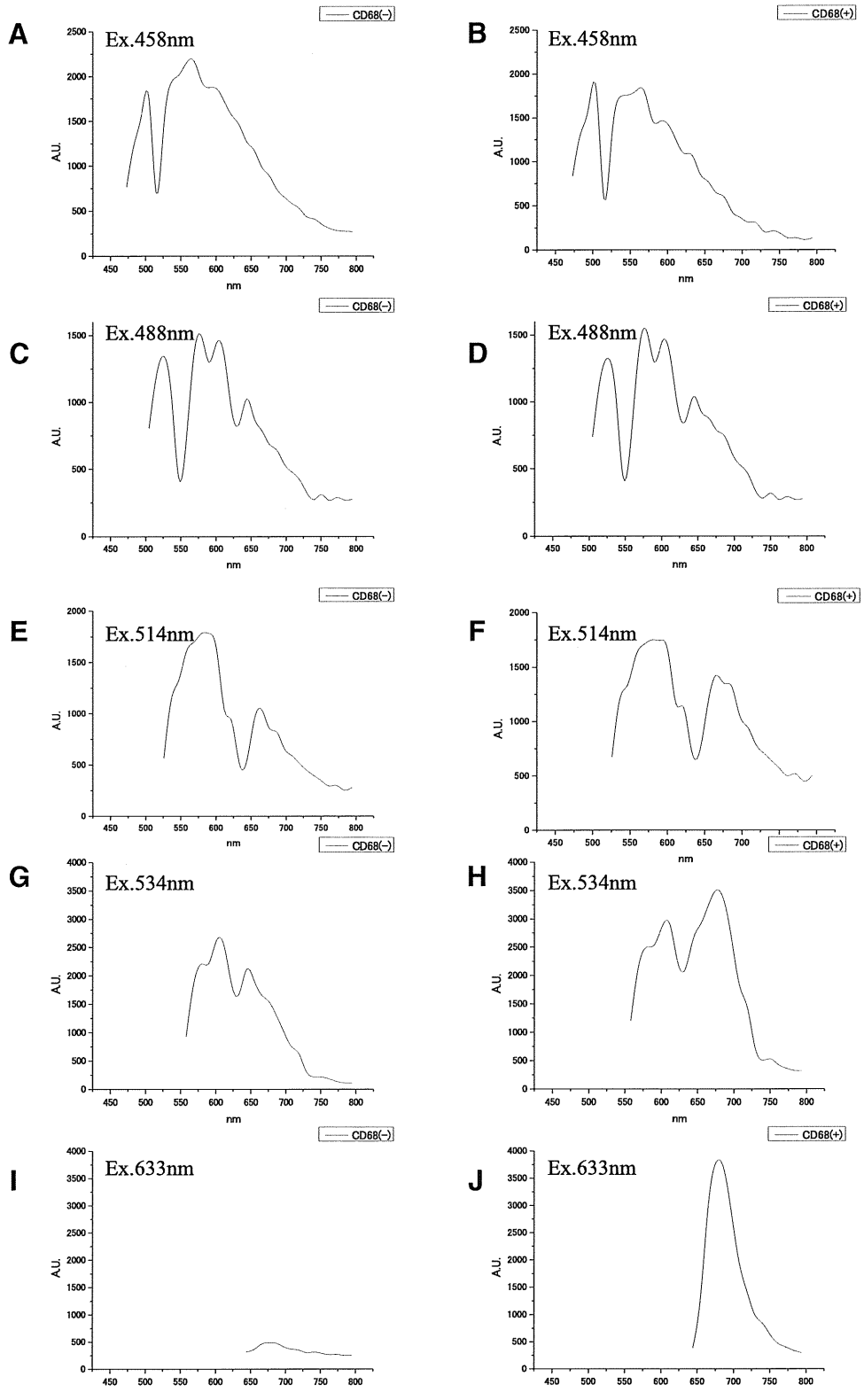

FIGURE 6. Fluorescence emission fingerprints of CD68-negative and -positive cells collected from subretinal fluid in the eye with rhegmatogenous retinal detachment. (**A**, **C**, **E**, **G**, **I**) the CD68-negative cells; (**B**, **D**, **F**, **H**, **J**) the CD68-positive cells. Ex: Excitation wavelengths: 458, 488, 514, 534, and 633 nm, respectively (*top* to *bottom*).

late in the macrophages. Specifically, the accumulated outer segment material in phagosomes in the macrophages may generate autofluorescence similar to that in the retinal pigment epithelium. Since the former two types of cells showed autofluorescence in the cells, they were considered to be the source of subretinal autofluorescence in part. Autofluorescence was observed in the phagosomal vacuole. Hence, autofluorescent substances may have already been synthesized in shed outer segments before phagocytosis. Recent reports have also raised this possibility.[14,39] However, autofluorescence characteristics of shed substances in the subretinal space are still unknown. Further study is needed of this phenomenon.

The digested photoreceptor outer segments that may not be properly processed in the macrophages may become lipofuscin. The possibility of the photoreceptor outer segments being

TABLE 2. Peak Analysis of the 50 Inclusions in the CD68-negative and -positive Cells

Emission Wavelength (NM)	CD68	Excitation Wavelength (nm) 458 (−)	458 (+)	488 (−)	488 (+)	514 (−)	514 (+)	543 (−)	543 (+)	633 (−)	633 (+)
462		0	—	—	—	—	—	—	—	—	—
473		0	0	—	—	—	—	—	—	—	—
483		0	0	—	—	—	—	—	—	—	—
494		3	0	—	—	—	—	—	—	—	—
505		45	50	0	0	—	—	—	—	—	—
515		0	0	0	0	—	—	—	—	—	—
526		0	0	50	50	0	0	—	—	—	—
537		2	1	0	0	0	0	—	—	—	—
547		1	1	0	0	0	0	—	—	—	—
558		39	33	0	0	1	0	0	0	—	—
569		8	16	0	0	4	5	0	0	—	—
580		0	0	39	44	21	25	0	1	—	—
590		0	0	0	0	25	20	0	0	—	—
601		0	0	11	6	0	0	29	23	—	—
612		0	0	0	0	0	0	21	27	—	—
622		0	0	0	0	0	0	0	0	—	—
633		0	0	0	0	0	0	0	0	—	—
644		0	0	45	50	0	0	46	1	0	0
654		0	0	0	0	1	0	3	0	0	0
665		0	0	0	0	49	49	0	0	0	0
676		0	0	0	0	0	1	0	50	47	50
687		0	0	0	0	0	0	0	0	3	0
697		0	0	0	0	0	0	0	0	0	0
708		0	0	0	0	0	0	0	0	0	0
‖		‖	‖	‖	‖	‖	‖	‖	‖	‖	‖
794		0	0	0	0	0	0	0	0	0	0

processed into autofluorescent material in the subretinal macrophages could not be excluded.

CD68-positive cells showed two autofluorescence peaks within the range of 480 to 750 nm. In the present study, green emission peaks of autofluorescence, 505 nm for 457-nm excitation and 526 nm for 488-nm excitation, were observed. This emission spectrum was reported to appear in living human eyes.[37,40] Flavin adenine dinucleotide (FAD) is considered to be the main source of the green emission. In the 488-nm emission spectra, the narrow peak appeared around 520 nm (Figs. 6C, 6D). A similar peak also appeared on the left shoulder of the broad peak (right), straddling 530 to 535 nm along the *x*-axis in the spectra induced by 458-nm light (Figs. 6A, 6B). The flavoprotein signal may be incorporated into this peak.[41] Since the green emission was not observed in macrophages in the lung[42] or peripheral blood,[43] the fluorophore would be distinctive to macrophages in the subretinal space. Why would this emission spectrum appear only in the inclusions of the macrophages in the subretinal space? Macrophages accumulate in the outer nuclear layer in regions of ongoing rod cell death after retinal detachment.[44] Degenerated photoreceptor cells may be phagocytized by the macrophages. The highest concentration of FAD is found in the mitochondria of the photoreceptor's inner segments. As the results of phagocytosis, the mitochondria of the photoreceptor cells may accumulate in the phagosomes of macrophages and show green emission autofluorescence. Therefore, the macrophages in the subretinal space in eyes with retinal detachment would be predicted to show that green and yellow autofluorescence originates from lipofuscin-like materials and FAD. Inclusions in cells of the mouse models of age-related macular degeneration showed a spectrum similar to that of our samples.[45] The increase in autofluorescence in an elderly population and patients with macular degeneration may reflect autofluorescence from macrophages associated with photoreceptor death.

In this study, we were unable to determine the chemical composition of autofluorescent substances, since the quantity of cells obtained from surgically removed subretinal fluid was limited. Further study is needed to examine whether the subretinal inclusions have the same composition as lipofuscin or FAD.

With regard to the origins of CD68-positive cells, we should use the other antibodies that are more specific for tissue macrophages. A minority of the retinal pigment epithelium has been reported to be CD68-positive in situ.[46] The transformation of the retinal pigment epithelium into the macrophages is assumed to be one source of the subretinal macrophages.[47] CD68-positive retinal pigment epithelial cells may look morphologically similar to macrophages. Therefore, the CD68-positive cells include the tissue macrophages and the transformed retinal pigment epithelium. To determine the contribution of the tissue macrophage to autofluorescence in the subretinal space, more specific staining is needed. However, the broad spectrum of autofluorescence and small amount of the specimens did not allow us to perform multiple staining. Further study of this issue is need.

In conclusion, we found that inclusions in the macrophages in the subretinal space emit intense autofluorescence. The spectra of the autofluorescence are very similar to that of the retinal pigment epithelium. Hence, autofluorescent properties of deposits in subretinal space raise the possibility that they are macrophages, and further critical markers are needed for clinical assessment as to their identity.

References

1. Eldred GE, Lasky MR. Retinal age pigments generated by self-assembling lysosomotropic detergents. *Nature.* 1993;361:724–726.
2. Liu J, Itagaki Y, Ben-Shabat S, Nakanishi K, Sparrow JR. The biosynthesis of A2E, a fluorophore of aging retina, involves the for-

mation of the precursor, A2-PE, in the photoreceptor outer segment membrane. *J Biol Chem.* 2000;275:29354-29360.
3. Parish CA, Hashimoto M, Nakanishi K, Dillon J, Sparrow J. Isolation and one-step preparation of A2E and iso-A2E, fluorophores from human retinal pigment epithelium. *Proc Natl Acad Sci U S A.* 1998;95:14609-14613.
4. Spaide RF, Noble K, Morgan A, Freund KB. Vitelliform macular dystrophy. *Ophthalmology.* 2006;113:1392-1400.
5. Chung JE, Spaide RF. Fundus autofluorescence and vitelliform macular dystrophy. *Arch Ophthalmol.* 2004;122:1078-1079.
6. Framme C, Walter A, Gabler B, Roider J, Sachs HG, Gabel VP. Fundus autofluorescence in acute and chronic-recurrent central serous chorioretinopathy. *Acta Ophthalmol Scand.* 2005;83:161-167.
7. Kon Y, Iida T, Maruko I, Saito M. The optical coherence tomography-ophthalmoscope for examination of central serous chorioretinopathy with precipitates. *Retina.* 2008;28:864-869.
8. Maruko I, Iida T, Ojima A, Sekiryu T. Subretinal dot-like precipitates and yellow material in central serous chorioretinopathy. *Retina.* 2011;31:759-765.
9. Sasamoto Y, Gomi F, Sawa M, Tsujikawa M, Hamasaki T. Macular pigment optical density in central serous chorioretinopathy. *Invest Ophthalmol Vis Sci.* 2010;51:5219-5225.
10. Sekiryu T, Iida T, Maruko I, Saito K, Kondo T. Infrared fundus autofluorescence and central serous chorioretinopathy. *Invest Ophthalmol Vis Sci.* 2010;51:4956-4962.
11. Spaide RF, Klancnik JM Jr. Fundus autofluorescence and central serous chorioretinopathy. *Ophthalmology.* 2005;112:825-833.
12. Shields CL, Bianciotto C, Pirondini C, Materin MA, Harmon SA, Shields JA. Autofluorescence of orange pigment overlying small choroidal melanoma. *Retina.* 2007;27:1107-1111.
13. Koizumi H, Maruyama K, Kinoshita S. Blue light and near-infrared fundus autofluorescence in acute Vogt-Koyanagi-Harada disease. *Br J Ophthalmol.* 2010;94:1499-1505.
14. Spaide R. Autofluorescence from the outer retina and subretinal space: hypothesis and review. *Retina.* 2008;28:5-35.
15. Weingeist TA, Kobrin JL, Watzke RC. Histopathology of Best's macular dystrophy. *Arch Ophthalmol.* 1982;100:1108-1114.
16. Schachat AP, de la Cruz Z, Green WR, Patz A. Macular hole and retinal detachment in Best's disease. *Retina.* 1985;5:22-25.
17. Kamei M, Yoneda K, Kume N, et al. Scavenger receptors for oxidized lipoprotein in age-related macular degeneration. *Invest Ophthalmol Vis Sci.* 2007;48:1801-1807.
18. Grossniklaus HE, Miskala PH, Green WR, et al. Histopathologic and ultrastructural features of surgically excised subfoveal choroidal neovascular lesions: submacular surgery trials report no. 7. *Arch Ophthalmol.* 2005;123:914-921.
19. Herbert EN, Sheth HG, Wickremasinghe S, Luthert PJ, Bainbridge J, Gregor ZJ. Nature of subretinal fluid in patients undergoing vitrectomy for macular hole: a cytopathological and optical coherence tomography study. *Clin Exp Ophthalmol.* 2008;36:812-816.
20. Baudouin C, Hofman P, Brignole F, Bayle J, Loubiere R, Gastaud P. Immunocytology of cellular components in vitreous and subretinal fluid from patients with proliferative vitreoretinopathy. *Ophthalmologica.* 1991;203:38-46.
21. Kremer I, Nissenkorn I, Ben-Sira I. Cytologic and biochemical examination of the subretinal fluid in diagnosis of Coats' disease. *Acta Ophthalmol (Copenh).* 1989;67:342-346.
22. Lai WW, Leung GY, Chan CW, Yeung IY, Wong D. Simultaneous spectral domain OCT and fundus autofluorescence imaging of the macula and microperimetric correspondence after successful repair of rhegmatogenous retinal detachment. *Br J Ophthalmol.* 2010;94:311-318.
23. Ojima A, Iida T, Sekiryu T, Maruko I, Sugano Y. Photopigments in central serous chorioretinopathy. *Am J Ophthalmol.* 2011;151:940-952 e941.
24. Miller SA. Fluorescence in Best's vitelliform dystrophy, lipofuscin, and fundus flavimaculatus. *Br J Ophthalmol.* 1978;62:256-260.
25. Delori FC, Fleckner MR, Goger DG, Weiter JJ, Dorey CK. Autofluorescence distribution associated with drusen in age-related macular degeneration. *Invest Ophthalmol Vis Sci.* 2000;41:496-504.
26. Ramasubramanian A, Shields CL, Harmon SA, Shields JA. Autofluorescence of choroidal hemangioma in 34 consecutive eyes. *Retina.* 2010;30:16-22.
27. Vogt A. Ueber subvaskulare Weissfleckung der abgelosten retina, von der Form von weissen Prazipitaten. *Klin Monatsbl Augenheilkd,* 1938;101:864-866.
28. Robertson DM. Delayed absorption of subretinal fluid after scleral buckling procedures: the significance of subretinal precipitates. *Trans Am Ophthalmol Soc.* 1978;76:557-583.
29. Toti P, Morocutti A, Sforzi C, De Santi MM, Catella AM, Baiocchi S. The subretinal fluid in retinal detachment: a cytologic study. *Doc Ophthalmol.* 1991;77:39-46.
30. Shields JA, Shields CL. Review: coats disease: the 2001 LuEsther T. Mertz lecture. *Retina.* 2002;22:80-91.
31. Haik BG, Koizumi J, Smith ME, Ellsworth RM. Fresh preparation of subretinal fluid aspirations in Coats' disease. *Am J Ophthalmol.* 1985;100:327-328.
32. Matsumura M, Yamakawa R, Yoshimura N, Shirakawa H, Okada M, Ogino N. Subretinal strands: tissue culture and histological study. *Graefes Arch Clin Exp Ophthalmol.* 1987;225:341-345.
33. Mietz H, Stodtler M, Wiedemann P, Heimann K. Immunohistochemistry of cellular proliferation in eyes with longstanding retinal detachment. *Int Ophthalmol.* 1994;18:329-337.
34. Okada M, Ogino N, Matsumura M, Honda Y, Nagai Y. The process of subretinal strand formation. *Jpn J Ophthalmol.* 1992;36:222-234.
35. Trese MT, Chandler DB, Machemer R. Subretinal strands: ultrastructural features. *Graefes Arch Clin Exp Ophthalmol.* 1985;223:35-40.
36. Delori FC, Dorey CK, Staurenghi G, Arend O, Goger DG, Weiter JJ. In vivo fluorescence of the ocular fundus exhibits retinal pigment epithelium lipofuscin characteristics. *Invest Ophthalmol Vis Sci.* 1995;36:718-729.
37. Boulton M, Docchio F, Dayhaw-Barker P, Ramponi R, Cubeddu R. Age-related changes in the morphology, absorption and fluorescence of melanosomes and lipofuscin granules of the retinal pigment epithelium. *Vision Res.* 1990;30:1291-1303.
38. Haralampus-Grynaviski NM, Lamb LE, Clancy CM, et al. Spectroscopic and morphological studies of human retinal lipofuscin granules. *Proc Natl Acad Sci U S A.* 2003;100:3179-3184.
39. Sparrow JR, Wu Y, Nagasaki T, Yoon KD, Yamamoto K, Zhou J. Fundus autofluorescence and the bisretinoids of retina. *Photochem Photobiol Sci.* 2010;9:1480-1489.
40. Elner SG, Elner VM, Field MG, Park S, Heckenlively JR, Petty HR. Retinal flavoprotein autofluorescence as a measure of retinal health. *Trans Am Ophthalmol Soc.* 2008;106:215-222; discussion 222-214.
41. Benson RC, Meyer RA, Zaruba ME, McKhann GM. Cellular autofluorescence: is it due to flavins? *J Histochem Cytochem.* 1979;27:44-48.
42. Pauly JL, Allison EM, Hurley EL, Nwogu CE, Wallace PK, Paszkiewicz GM. Fluorescent human lung macrophages analyzed by spectral confocal laser scanning microscopy and multispectral cytometry. *Microsc Res Tech.* 2005;67:79-89.
43. Davis RW, Timlin JA, Kaiser JN, Sinclair MB, Jones HD, Lane TW. Accurate detection of low levels of fluorescence emission in autofluorescent background: francisella-infected macrophage cells. *Microsc Microanal.* 2010;16:478-487.
44. Nakazawa T, Takeda M, Lewis GP, et al. Attenuated glial reactions and photoreceptor degeneration after retinal detachment in mice deficient in glial fibrillary acidic protein and vimentin. *Invest Ophthalmol Vis Sci.* 2007;48:2760-2768.
45. Xu H, Chen M, Manivannan A, Lois N, Forrester JV. Age-dependent accumulation of lipofuscin in perivascular and subretinal microglia in experimental mice. *Aging Cell.* 2008;7:58-68.
46. Elner SG, Elner VM, Nielsen JC, Torczynski E, Yu R, Franklin WA. CD68 antigen expression by human retinal pigment epithelial cells. *Exp Eye Res.* 1992;55:21-28.
47. Mandelcorn MS, Machemer R, Fineberg E, Hersch SB. Proliferation and metaplasia of intravitreal retinal pigment epithelium cell autotransplants. *Am J Ophthalmol.* 1975;80:227-237.

Photopigments in Central Serous Chorioretinopathy

AKIRA OJIMA, TOMOHIRO IIDA, TETSUJU SEKIRYU, ICHIRO MARUKO, AND YUKINORI SUGANO

• PURPOSE: To investigate functional abnormalities in eyes with central serous chorioretinopathy (CSC).
• DESIGN: Observational case series.
• METHODS: Sixteen eyes with CSC were enrolled. Autofluorescence densitometry was performed to measure the optical density of the photopigments. Serial fundus autofluorescence (FAF) images were obtained by Heidelberg Retina Angiogram 2. We calculated the autofluorescence optical density difference from the FAF images. To compare the distribution pattern of autofluorescence optical density difference to the findings of outer retina, spectral-domain optical coherence tomography (SD-OCT) was performed in the acute phase and after resolution of CSC.
• RESULTS: The autofluorescence optical density difference decreased at the serous retinal detachment (SRD) in all 16 eyes. After resolution, the photoreceptor inner and outer segment junction (IS/OS) was irregular in 13 eyes and defective in 3 eyes on SD-OCT. The autofluorescence optical density difference did not improve in any eyes. Five eyes were reexamined 3 month after resolution. In 4 of the 5 eyes, SD-OCT showed that the IS/OS was well delineated and 1 eye defective. The autofluorescence optical density difference improved in 2 of the 4 eyes, but not in the other 2 eyes. In the 1 eye without well-delineated IS/OS, the autofluorescence optical density difference did not improve.
• CONCLUSION: In eyes with CSC, the photopigment density decreased at the SRD. The density remained decreased immediately after resolution and showed delayed recovery. The photopigments decreased even in eyes with morphologic recovery of the outer retina. (Am J Ophthalmol 2011;151:940–952. © 2011 by Elsevier Inc. All rights reserved.)

CENTRAL SEROUS CHORIORETINOPATHY (CSC) IS characterized by serous retinal detachment (SRD) in the macular area. Focal dye leakage at the level of the retinal pigment epithelium (RPE) is seen on fluorescein angiography. In most eyes, the SRD resolves spontaneously, and the visual acuity (VA) recovers fully in these eyes. However, patients often complain about relative scotoma, abnormal color sensation, and micropsia despite resolution of the SRD.

Accepted for publication Dec 3, 2010.

From the Department of Ophthalmology, Fukushima Medical University School of Medicine, Fukushima, Japan.

Inquiries to Akira Ojima, Department of Ophthalmology, Fukushima Medical University School of Medicine, 1 Hikarigaoka, Fukushima, Japan; e-mail: ao@fmu.ac.jp

Morphologic retinal abnormalities in CSC have been observed on optical coherence tomography (OCT).[1–8] In the acute phase of CSC, thickened neurosensory retina and elongated photoreceptor outer segments are seen at the area of the SRD.[1–8] In the quiescent phase, defects of the photoreceptor inner and outer segment junction (IS/OS) are sometimes seen.[4] Thinning of the outer photoreceptor layer and the defects in the subfoveal IS/OS may be associated with VA loss.[2,4,8]

Some studies using microperimetry have reported that retinal sensitivity was attenuated in eyes with CSC even after resolution of the SRD.[9,10] Spectral-domain OCT (SD-OCT) showed loss of retinal sensitivity in areas with an irregular RPE or a defect of the IS/OS.[10] Reduced amplitudes of the multifocal electroretinogram were observed not only in the acute phase but also after resolution of the SRD.[11,12] Although these functional disorders seem to be associated with loss of the IS/OS or RPE atrophy, some patients complain about blurred vision even after complete morphologic recovery of the IS/OS. The role of the OCT findings in visual function is uncertain. In these cases, functional impairment might be attributed to decreases in the visual photopigments.

Retinal densitometry is the only objective method for investigating visual photopigments in vivo.[13–22] Liem and associates,[23] using reflective densitometry in eyes with CSC, reported that the rhodopsin concentration decreased in the area of the SRD. Since that method requires special equipment, it is not used clinically.

In a previous study, we reported other methods of retinal densitometry using the fundus autofluorescence (FAF) examination by commercially available scanning laser ophthalmoscope.[24] We recorded serial FAF images using the Heidelberg Retina Angiogram 2 (HRA2; Heidelberg Engineering, Dossenheim, Germany), and calculated the photopigment density from the time-dependent changes in intensity of FAF during excitation. We named the technique autofluorescence densitometry. The density is measured as the autofluorescence optical density difference of the photopigments. This new technique can examine a much broader macular area than in previous studies and create a distribution map of optical density of the photopigments. It is also easy to compare the distributions of the photopigment densities with other retinal imaging devices such as SD-OCT. We used autofluorescence densitometry to evaluate changes in the photopigments in acute and quiescent phase of CSC.

0002-9394/$36.00
doi:10.1016/j.ajo.2010.12.005

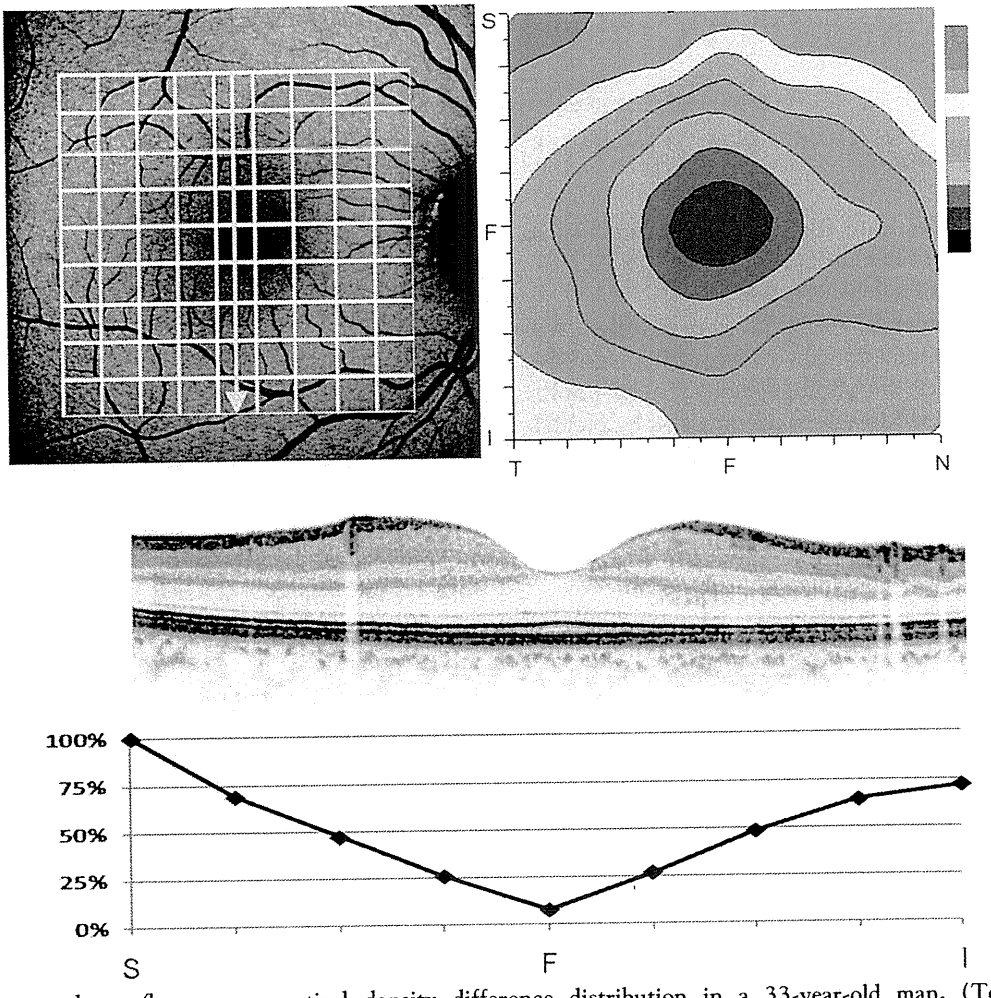

FIGURE 1. A normal autofluorescence optical density difference distribution in a 33-year-old man. (Top left) Fundus autofluorescence image. The intensity of each point on the grids was measured to calculate the autofluorescence optical density difference. The arrow indicates the line of the spectral-domain optical coherence tomography (SD-OCT) scan. (Top right) A normal autofluorescence optical density difference map has a concentric pattern. S = superior; F = fovea; I = inferior; T = temporal; N = nasal. (Middle) A vertical SD-OCT scan shows a normal layer structure. (Bottom) The % autofluorescence optical density difference graph at the SD-OCT scan line. The abscissa indicates the position.

METHODS

AMONG 26 CONSECUTIVE PATIENTS WITH CSC EXAMINED by both autofluorescence densitometry and SD-OCT, 16 eyes of 16 patients were included in this study (14 men, 2 women; mean age, 50.1 years; range, 31–71 years). All patients visited the Department of Ophthalmology at Fukushima Medical University Hospital between August 1, 2008 and May 31, 2009. The 16 eyes met the following criteria: the maximum diameter of the SRD exceeded 3 disc diameters including the fovea; autofluorescence densitometry was performed during the acute and quiescent phases; and resolution of the SRD was observed on SD-OCT during the follow-up period. The remaining 10 patients did not meet these criteria. In the 10 patients who were excluded, 8 patients had small SRD with maximum diameter less than 3 disc diameters, and 2 patients could not be followed up.

All patients underwent a comprehensive ophthalmologic examination, including measurement of the best-corrected VA, slit-lamp biomicroscopy, fundus photography, fluorescein angiography, SD-OCT, and FAF. The best-corrected VA was measured with a Japanese standard decimal visual chart and converted to logarithm of the minimal angle of resolution for statistical analysis. SD-OCT was performed with a 3-dimensional OCT system (Topcon, Tokyo, Japan) or Spectralis OCT system (Heidelberg Engineering, Heidelberg, Germany). The diagnosis of CSC was confirmed by the presence of a macular SRD and leakage from the level of the RPE on fluorescein angiography. Patients with other pathologies that can cause retinal detachment, such as age-related macular degeneration, Harada's disease, posterior scleritis, and any other macular diseases, were excluded. All data were collected prospectively and reviewed in a masked fashion.

We also examined 10 control subjects (mean age, 40 years; age range, 31–55 years) who were free from retinal

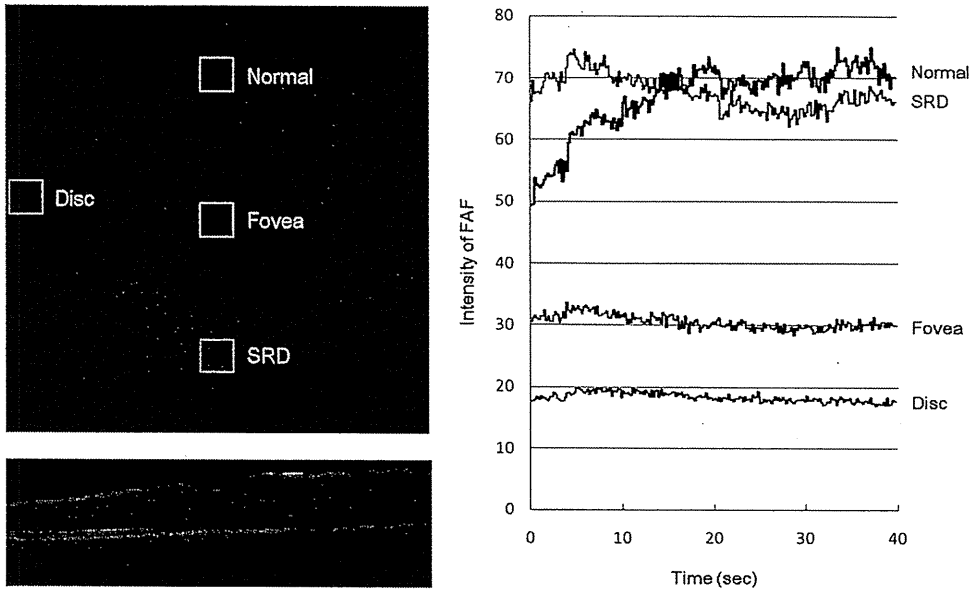

FIGURE 2. Changes in fundus autofluorescence (FAF) intensity in the left eye of a 37-year-old man with acute central serous chorioretinopathy (Patient 4). (Top left) FAF image. The mean intensity within each area was measured. The squares indicate the area of measurement. Normal, the area without a serous retinal detachment (SRD); SRD, the area within an SRD. (Bottom left) A vertical spectral-domain optical coherence tomography scan shows an SRD. (Right) Time-dependent changes in the FAF intensity during light exposure. The intensity increased in the normal area because of bleaching of the retina. The area with an SRD does not have increased FAF. The increases in FAF intensity indicate the presence of normal photopigments. The change in intensity is low at the fovea, because the excitation light is attenuated by macular pigment. The autofluorescence optical density difference cannot be evaluated accurately at the fovea. The FAF intensity is very low and does not change by light exposure at the disc.

diseases, significant cataract, or corneal opacity. All subjects underwent the same examination as above except for fluorescein angiography.

Patients who needed good vision because of their occupations or desired treatment underwent laser photocoagulation after being informed of the risks and benefits. Treatment was performed using a DPSS yellow laser (561 nm; Nidek, Gamagori, Japan) with a spot size of 200 μm, power of 70 to 100 mW, and application time of 0.20 second. The endpoint of laser photocoagulation was slight graying of the RPE.

The autofluorescence optical density difference of the photopigments was measured repeatedly by the autofluorescence densitometry technique of the FAF examination to investigate time-dependent changes. We also evaluated the morphologic changes of the outer retina on the horizontal and vertical images of the SD-OCT. The area of interest was examined by raster scan. We classified the OCT findings of IS/OS in the area of SRD into 3 groups: clear, irregular, and defect. "Clear" indicates normal IS/OS line; "irregular" is discontinuous or blurred IS/OS line; "defect" means lack of IS/OS line.

The autofluorescence densitometry technique was described previously.[19] The FAF images were recorded using HRA2. After pupil dilation with topical tropicamide and phenylephrine, the patients were dark-adapted for at least 30 minutes before the examination. Serial FAF images were obtained over 40 seconds using high-speed movie mode. The angle of field was 30 degrees. The intensity of excitation was 100% and the gain was 94%. The FAF images were aligned to fix the viewpoint using the software in the HRA2 system and were output as audio video interleaved (AVI) files for measurement. We measured the distribution of the FAF intensity in a 6 × 6-mm-square area around the fovea. The area was divided into 9 × 9 grids, and the intensity of each point was measured as an 8-bit grayscale value on the frame of the AVI files (Gray-val; Library Inc, Tokyo, Japan).

To estimate the autofluorescence optical density difference of the photopigments, the grayscale value during light exposure was fitted to the following formula. The intensity of the FAF at time t was described as:

$$\log[F(t)] = \log[F(\infty)] - fODD \times \exp(-kt)$$

where F(t) is the measured autofluorescence at time t, F(∞) is the autofluorescence at an infinite time when the F(t) approaches a constant level, fODD is the optical density difference of the pigment between the dark-adapted density and the density of the pigment after an infinitely long duration, and k is the time constant relating the chromophore properties and the intensity of light at the measurement site. We fitted the value of the FAF intensity to the equation on a least-squares basis with the Levenberg-Marquardt method, which provides the 3 unknown parameters (log[F(∞)], fODD, and k), using Origin 8.0 computer software (OriginLab Corporation,

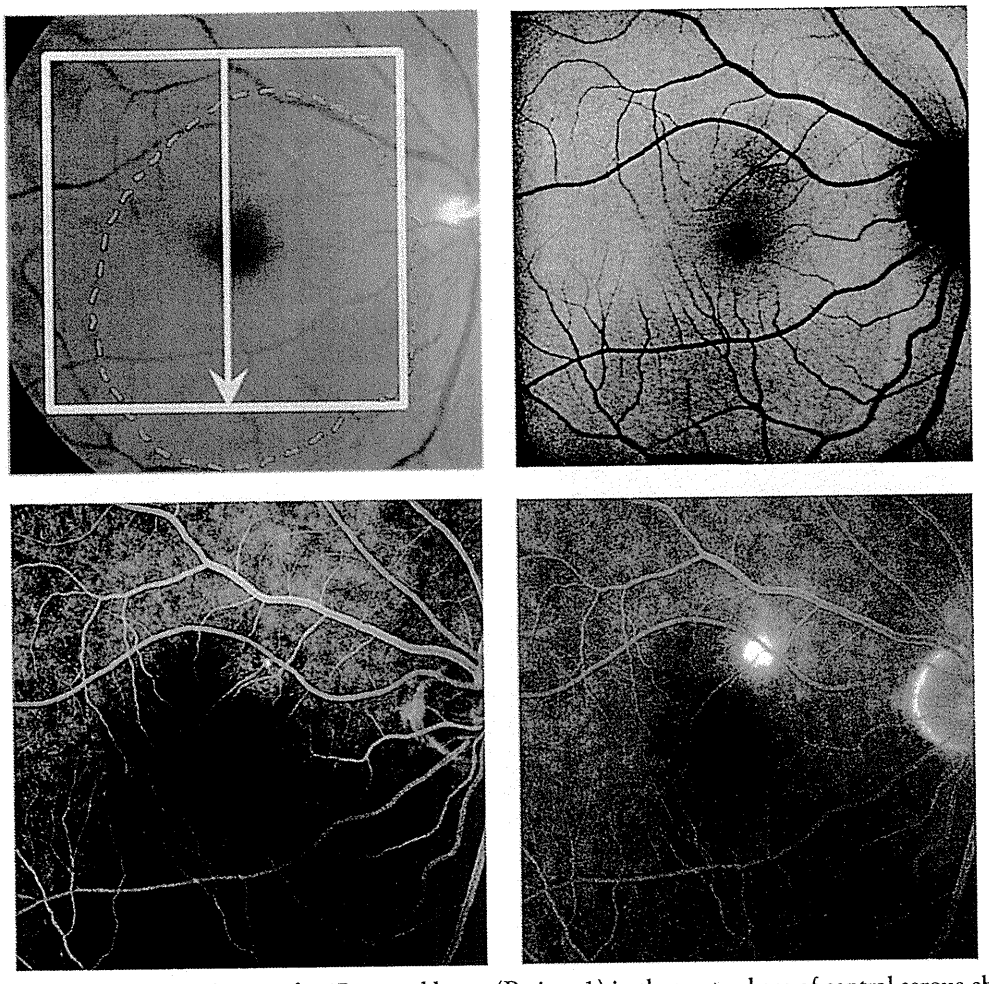

FIGURE 3. Fundus images of the right eye of a 47-year-old man (Patient 1) in the acute phase of central serous chorioretinopathy. (Top left) Fundus photograph. The square indicates the area in which the autofluorescence optical density difference was measured (see Figure 4). The dashed line shows the area of the serous retinal detachment. The yellow arrow indicates the scanning line of spectral-domain optical coherence tomography (see Figure 4). (Top right) Fundus autofluorescence image. (Bottom) Focal dye leakage is seen in (Bottom left) the early phase and (Bottom right) the late phase of the fluorescein angiograms.

Northampton, Massachusetts, USA). The results were displayed using a contour map classified into 11 phases (autofluorescence optical density difference map). When the intensity of the autofluorescence decreased or the change in the autofluorescence intensity was too small to fit the equation at the measurement site, the autofluorescence optical density difference of the site was treated as zero.

RESULTS

THE TABLE SHOWS THE CLINICAL PATIENT PROFILES. THE duration of symptoms from the subjective onset ranged from 1 to 49 months (mean, 10.4 months). Six patients with symptom duration of more than 6 months were diagnosed with chronic CSC. The other 16 patients were diagnosed with acute CSC.

In the current study, we observed all 16 eyes in the acute phase and immediately after resolution of the SRD. Five of the 16 eyes were reexamined 3 months after resolution. All eyes in the acute phase had focal leakage at the macular area on fluorescein angiography and a SRD that included the fovea. Eleven of the 16 eyes had an elongated photoreceptor outer segment on SD-OCT. Twelve of the 16 eyes were treated with laser photocoagulation. The SRDs resolved on SD-OCT between 3 and 54 months (mean, 13.4 months) from the subjective onset of symptoms.

The autofluorescence optical density difference map showed a concentric pattern in all 10 control subjects. Figure 1 shows a normal autofluorescence optical density difference map of a healthy subject (33-year-old man). All FAF and SD-OCT findings were normal (Figure 1, Top left, Middle). To calculate the autofluorescence optical density difference, time-dependent changes in the FAF

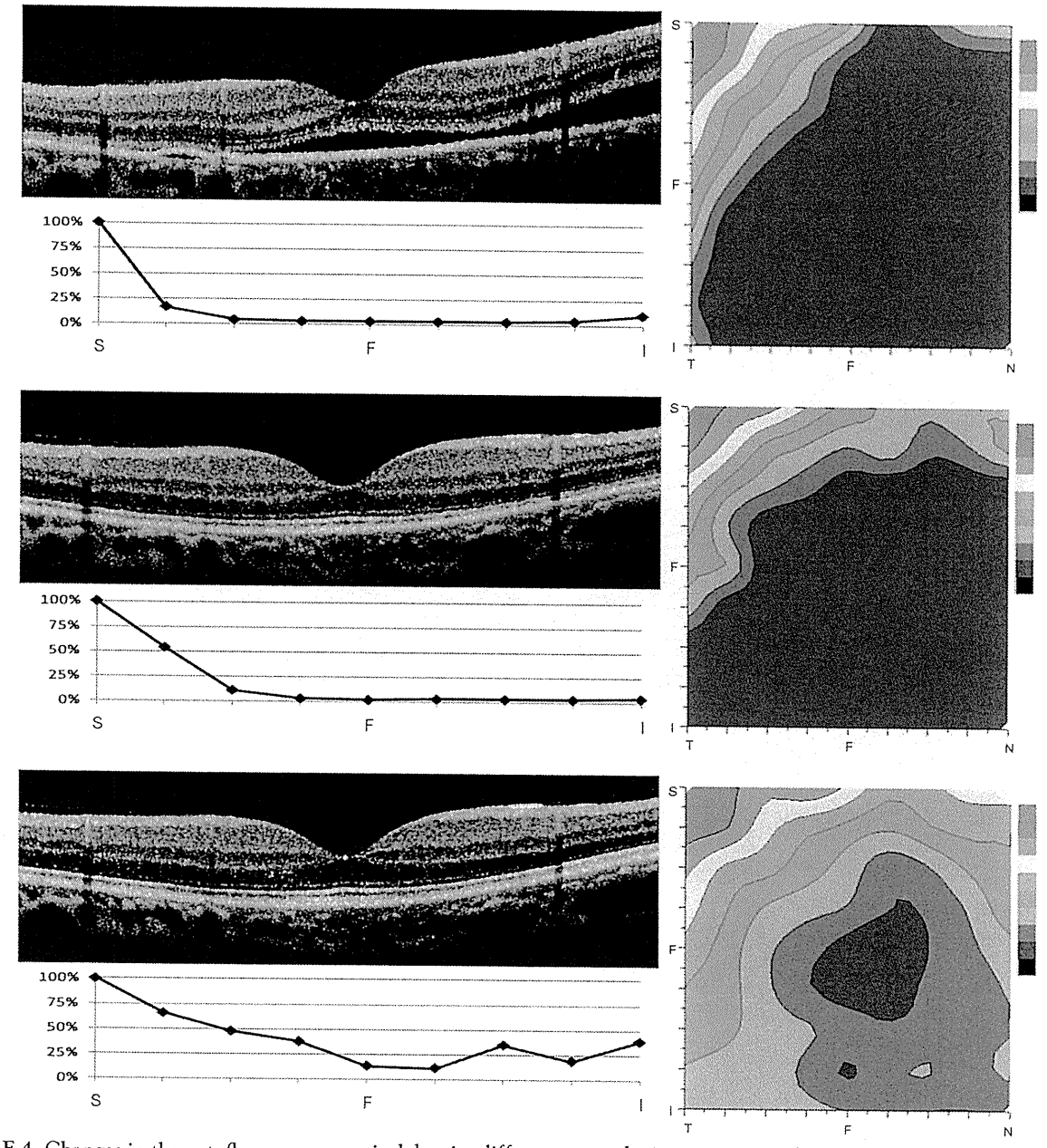

FIGURE 4. Changes in the autofluorescence optical density difference map during acute central serous chorioretinopathy of Patient 1. (Top) Spectral-domain optical coherence tomography (SD-OCT) and autofluorescence densitometry in the acute phase. A vertical SD-OCT scan shows that a serous retinal detachment (SRD) has spread widely within the vascular arcade. Two-dimensional mapping of the autofluorescence optical density difference demonstrates that the concentricity is disrupted. An area of low autofluorescence optical density difference corresponds to the SRD. The % autofluorescence optical density difference graph at the SD-OCT scan line shows that the autofluorescence optical density difference is lower at the SRD than the unaffected area. The abscissa indicates the position: S = superior; F = fovea; I = inferior. (Middle) SD-OCT and autofluorescence densitometry immediately after resolution. The SRD has resolved and the photoreceptor inner and outer segment junction (IS/OS) line disappeared at the affected area on SD-OCT. The concentricity of the autofluorescence optical density difference map did not improve compared to the acute phase. The % autofluorescence optical density difference has not improved at the affected area. (Bottom) Three months after reattachment. The IS/OS line is clearly delineated at the affected area on SD-OCT. The autofluorescence optical density difference map recovers concentricity. The % autofluorescence optical density difference has increased compared with the previous measurement but not to the level of the unaffected area.

intensity inside 9 × 9 grids were measured (Figure 1, Top left). Each grid was 60 × 60 pixels. The autofluorescence optical density difference map showed a normal concentric pattern (Figure 1, Top right). As the wavelength of the excitation light was 488 nm, the map mainly represented the distribution of rhodopsin.[24]

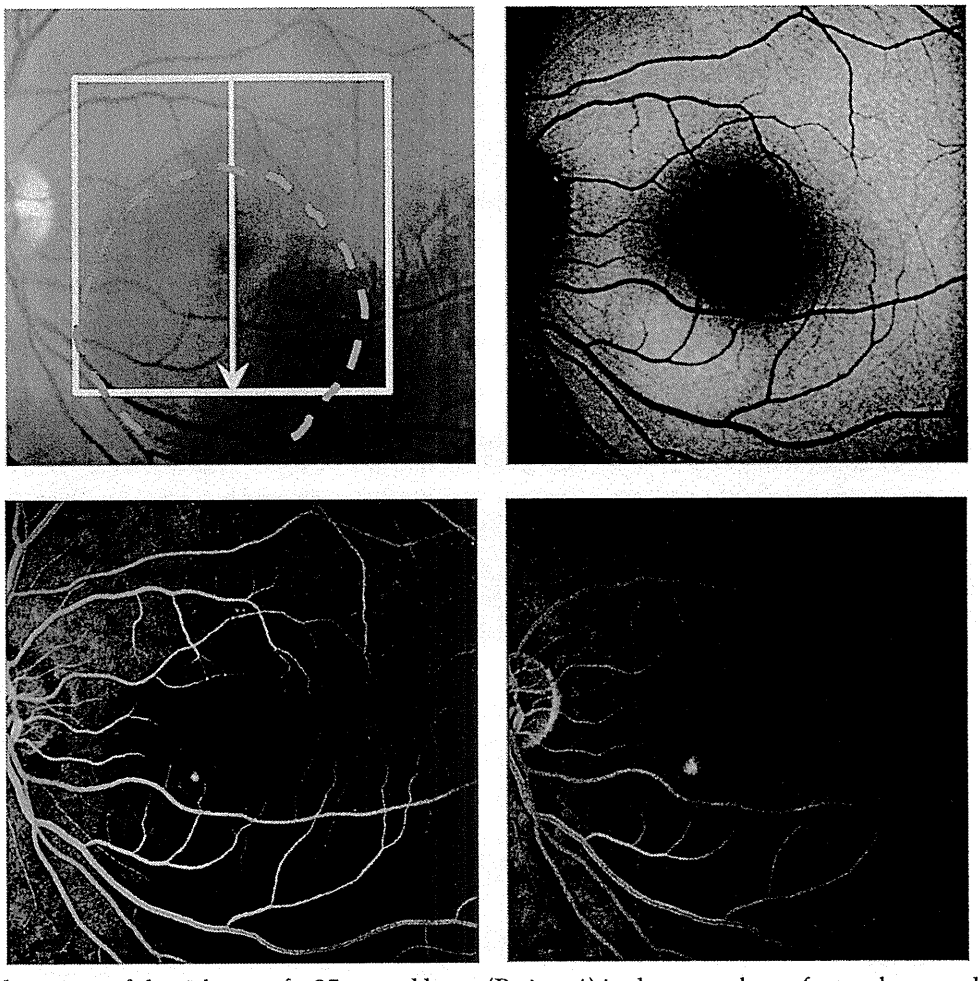

FIGURE 5. Fundus images of the right eye of a 37-year-old man (Patient 4) in the acute phase of central serous chorioretinopathy. (Top left) Fundus photograph. The square indicates the area in which the autofluorescence optical density difference was measured (see Figure 6). The dashed line indicates the serous retinal detachment. The yellow arrow indicates the scanning line of spectral-domain optical coherence tomography (see Figure 6). (Top right) Fundus autofluorescence image. (Bottom) Focal dye leakage is seen in (Bottom left) the early phase and (Bottom right) the late phase of the fluorescein angiograms.

To evaluate the autofluorescence optical density difference at the affected area or to compare SD-OCT findings with autofluorescence optical density difference on the scanned line, we calculated the autofluorescence optical density difference percentage in each grid when the maximum value in the referred area was defined as 100% (% autofluorescence optical density difference). We defined the area in which the % autofluorescence optical density difference was 25% or lower as the low autofluorescence optical density difference area. Figure 1, Bottom shows the % autofluorescence optical density difference along the vertical scan of SD-OCT (Figure 1, Middle) in a representative case.

The photopigments decreased in the detached retina during excitation in acute CSC (Figure 2). Figure 2, Right indicates the time-dependent changes in intensity during light exposure at the corresponding normal area, the SRD, the fovea, and the disc. In the normal area, the retina was bleached and the intensity gradually increased to a plateau. However, the intensity did not increase in the SRD area, indicating a decrease in the photopigments at the detached retina. The intensity remained constant at the fovea and disc.

In the acute phase of eyes with an SRD on SD-OCT, the autofluorescence optical density difference map showed an eccentric pattern in all 16 eyes (Figures 3, 4, 5, and 6). An area of low autofluorescence optical density difference (dense blue) was broader than that in normal eyes, and the area corresponded to the SRD (Figure 4, Top, and Figure 6, Top). An area of high autofluorescence optical density difference (green, yellow, and orange) surrounded the area of low autofluorescence optical density difference. The % autofluorescence optical density difference also showed decrease in intensity corresponding to the area of the SRD on SD-OCT.

Immediately after resolution, the IS/OS was irregular in the area of SRD in 13 eyes and defective in 3 eyes on SD-OCT. In all 16 eyes, the area of low autofluorescence

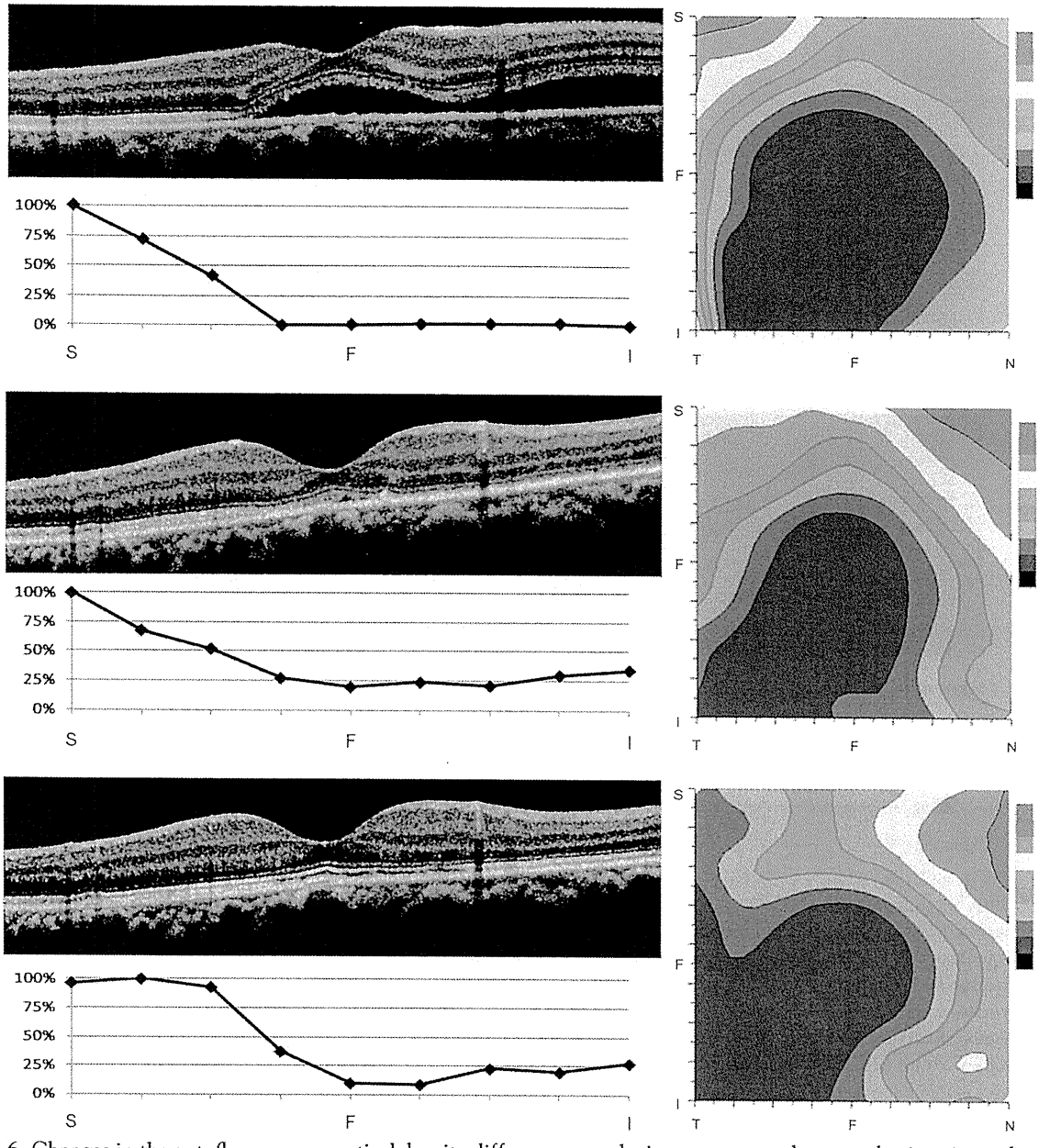

FIGURE 6. Changes in the autofluorescence optical density difference map during acute central serous chorioretinopathy of Patient 4. (Top) Spectral-domain optical coherence tomography (SD-OCT) and autofluorescence densitometry in the acute phase. A vertical SD-OCT scan shows a serous retinal detachment (SRD). Two-dimensional mapping of the autofluorescence optical density difference demonstrates that the concentricity is disrupted. An area of low autofluorescence optical density difference corresponds to the SRD. The % autofluorescence optical density difference graph at the SD-OCT scan line shows that the % autofluorescence optical density difference is lower at the SRD than the unaffected area. The abscissa indicates the position: S = superior; F = fovea; I = inferior. (Middle) SD-OCT and autofluorescence densitometry immediately after reattachment. The SRD has resolved and the photoreceptor inner and outer segment junction (IS/OS) line has disappeared at the affected area on SD-OCT. The autofluorescence optical density difference map has not improved compared to the acute phase. The % autofluorescence optical density difference has not improved at the affected area. (Bottom) Three months after reattachment. The IS/OS line is clearly delineated at the affected area on SD-OCT. The autofluorescence optical density difference mapping has not recovered its concentricity. The % autofluorescence optical density difference has increased compared with the previous measurement but not to the level of the unaffected area.

optical density difference was broader than normal, which was similar to the acute phase (Figure 4, Middle, and Figure 6, Middle). The autofluorescence optical density difference was comparably decreased in eyes with an irregular IS/OS and with a defective IS/OS. The % autofluorescence optical density difference on the same line of the SD-OCT scan also showed the decreased intensity (under 25%) at the reattached retina where the

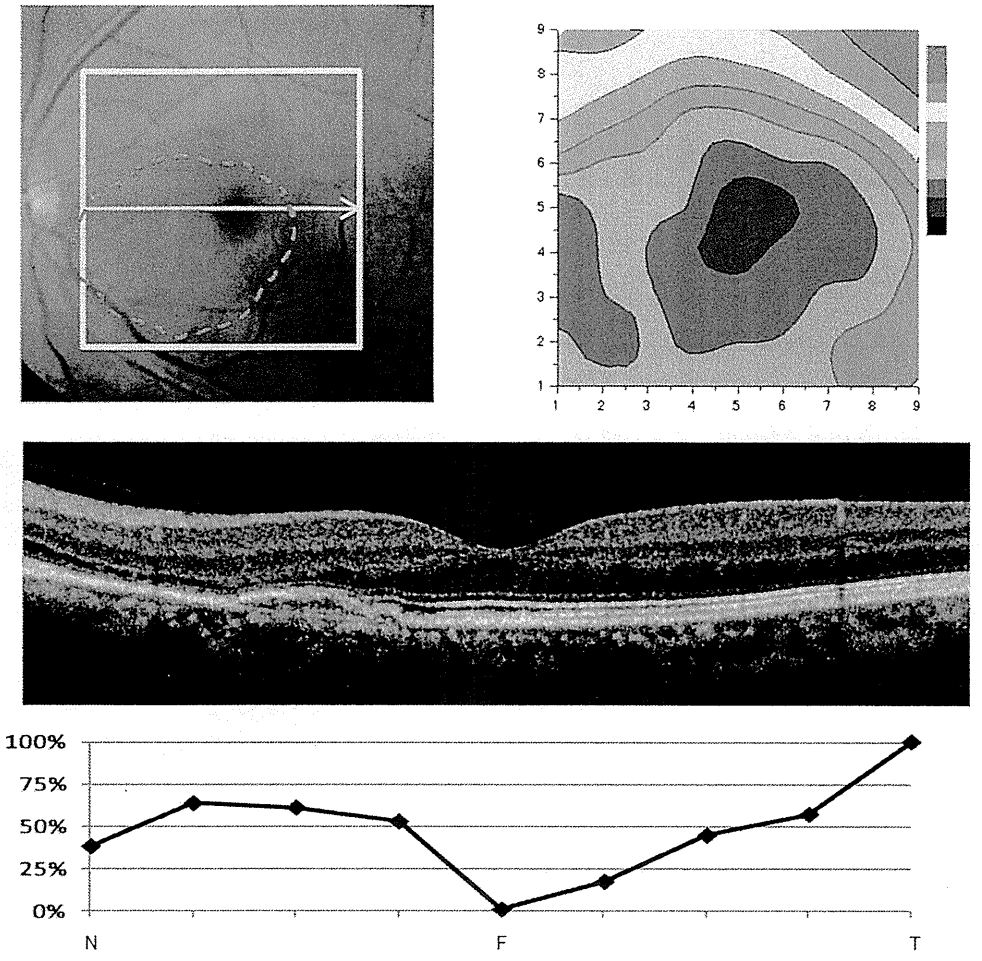

FIGURE 7. Fundus images of the left eye of a 56-year-old man (Patient 5) 3 months after resolution of central serous chorioretinopathy. (Top left) Fundus photograph. The square indicates the area in which the autofluorescence optical density difference was measured. The dashed line indicates the area where serous retinal detachment (SRD) was resolved. The yellow arrow indicates the scanning line of spectral-domain optical coherence tomography (SD-OCT). (Top right) The autofluorescence optical density difference map shows the disruption of concentricity of the photopigment density distribution. An area of low autofluorescence optical density difference corresponds to the affected area. (Middle) The SD-OCT scan shows resolution of serous retinal detachment. The photoreceptor inner and outer segment junction is defected at the reattached area. (Bottom) The % autofluorescence optical density difference graph at the SD-OCT scan line shows that the autofluorescence optical density difference decreased at the affected area. The abscissa indicates the position: N = nasal; F = fovea; T = temporal.

SD-OCT was irregular and the IS/OS was defective immediately after resolution of the SRD.

We performed autofluorescence densitometry and SD-OCT 3 months after resolution in 5 eyes (Patients 1, 2, 3, 4, and 5). Four of the 5 eyes had a clearly delineated IS/OS. One eye had a defective IS/OS (Figure 7). In 2 of the 4 eyes with an IS/OS, the autofluorescence optical density difference map showed improved concentricity and the area of low autofluorescence optical density difference decreased, which indicated recovery of the photopigments (Figure 4, Bottom). The % autofluorescence optical density difference graph showed recovery at the reattached retina. In the other 2 eyes with an IS/OS, the autofluorescence optical density difference map showed eccentricity in the resolved area (Figure 6, Bottom). Although the subretinal fluid resolved and the IS/OS appeared clearly on the SD-OCT images in these 2 eyes, the % autofluorescence optical density difference graph showed lower percentages (under 25%) in the reattached retina compared to the normal area. The autofluorescence optical density difference map and the % autofluorescence optical density difference graph did not show recovery in the 1 eye without an IS/OS (Figure 7).

Figure 8 shows the number of grids of the 81 grids with a low autofluorescence optical density difference in all 16 eyes. There was no significant difference between the acute phase and immediately after resolution in 16 eyes. In the 5 eyes that were reexamined 3 months after resolution, the low autofluorescence optical density difference grids decreased in Cases 1 and 2, and the autofluorescence optical density difference improved in those 2 eyes. The low autofluorescence optical